2021•2022

Faculteit Industriële Ingenieurswetenschappen

master in de industriële wetenschappen: chemie

Masterthesis

Prediction of CO2 absorption in amine solutions via Machine Learning techniques

PROMOTOR :

Prof. dr. ir. Mumin Enis LEBLEBICI

BEGELEIDER :

De heer Ulderico DI CAPRIO

Frederik Vandael

Scriptie ingediend tot het behalen van de graad van master in de industriële wetenschappen: chemie

Gezamenlijke opleiding UHasselt en KU Leuven

UHASSELT KU LEUVEN

UHASSELT KU LEUVEN

2021•2022

Faculteit Industriële Ingenieurswetenschappen

master in de industriële wetenschappen: chemie

Masterthesis

Prediction of CO2 absorption in amine solutions via Machine Learning techniques

PROMOTOR :

Prof. dr. ir. Mumin Enis LEBLEBICI

BEGELEIDER :

De heer Ulderico DI CAPRIO

Frederik Vandael

Scriptie ingediend tot het behalen van de graad van master in de industriële wetenschappen: chemie

UHASSELT KU LEUVEN

Preface

This master's thesis is part of the joint industrial engineering program of the KULeuven and UHasselt. I would like to thank them, as well as the CIPT research group, for giving me the opportunity to conduct this research.

However this thesis would not be possible without the help of a few people. I want to thank Prof. dr. ir. Mumin Enis Leblebici for his input and feedback on this master's thesis. Secondly I want to thank my mentor Ulderico Di Caprio for his guidance during the lab work and the programming work of this thesis, and for his input and feedback. Further I would like to thank ir. Emine Kayahan for her help during the lab work and her input and feedback on the experimental results. Next I want to thank ing. Annelot Van den Bogaert and Jeroen Lievens for their input and feedback. Finally I want to thank my family for their continuous support during my studies.

Table of Contents

List of tables

Table of figures

Nomenclature

symbol	definition	unit
$K_G a_e$	volumetric mass transfer coefficient	$kmol.m^{-3}.kPa^{-1}.h^{-1}$
%wt	weight percentage	%
%vol	volume percentage	%
nAmine	total mol of amine	mol
nCO_2	total mol of CO2	mol
G_I	inert gas molar flux	$kmol.m^3.kPa^{-1}.h^{-1}$
P	total system pressure	kPa
yCO_2	molar fraction of CO2 in bulk gas	
y^*CO_2	molar fraction of CO2 in equilibrium with liuid and bulk concenctration	
YCO_2	molar ratio of CO2 in gas bulk	
h	height of the absorption zone	m
z	standard score	
u	mean	
s	standard deviation	
α_i	support vector	
b	bias	
d	degree	
γ	scaler	
c	regularization parameter	
ξ	soft margin	
ε	maximum error	

Abbreviations	
symbol	**definition**
artificial neural network	ANN
decision tree regressor	DTR
support vector regressor	SVR
support vector machine	SVM
monoethanolamine	MEA
N-methyldiethanolamine	MDEA
2-amino-2-mehtly-1-propanol	AMP
mean squared error	MSE
mean absolute error	MAE
International Panel on Climate Change	IPCC
carbon capture and storage	CCS
artificial intelligence	AI
machine learning	ML
polynomial kernel function	poly
linear kernel function	lin
radial basis kernel function	rbf
rectified linear unit	ReLU
hyperbolic tangent function	Tanh

Abstract

CO_2 capture in a spray column using amine solutions is one of the most promising techniques to reduce CO_2 emission, which is one of the causes of global warming. However, to applicate them on large scale an accurate model of the CO_2 capture process is needed. First-principle models have failed and the goal of this master's thesis is to create an accurate model of the CO_2 capture process using Machine Learning techniques. The trained models are: one artificial neural network (ANN), one decision tree regressor (DTR) and three support vector regressors (SVR). To train the models data points on monoethanolamine, 2-amino-2-methly-1-propanol and N-methyldiethanolamine were collected. Th model uses as input: the process conditions, information about the columns and the absorbent liquid. The output of the models is the K_Ga_e coefficient, which indicates the performance of the mass transfer. To compare the models to each other the R^2 score, MSE and MAE were calculated for each model, using the experimental K_Ga_e. The ANN model could not accurately predict the K_Ga_e, but showed potential for further improvement. The DTR model and SVR model with the linear kernel function are not able to make accurate prediction, the DTR model due to a lack of output variance and the SVR-lin due to the non-linearity relation between input and output. The SVR with the polynomial and radial basis kernel function were both able to accurately predict the K_Ga_e and were highly flexible both on process condition, spray technology and absorbent solutions.

Abstract in het Nederlands

CO_2 captatie in een sproeikolom met behulp van amineoplossingen is een van de meest beloftevolle technieken om de uitstoot van CO_2, een van de oorzaken van de opwarming van de aarde, te verminderen. Voor een implementatie op grote schaal is een nauwkeurig model van het CO_2 captatieproces nodig. First-principle modellen hebben gefaald en het doel van deze masterproef is om een nauwkeurig model te maken van het CO_2 captatieproces met behulp van Machine Learning technieken. De modellen zijn: een artificial neural network (ANN), een decision tree regressor (DTR) en drie support vector regressors (SVR). De modellen werden getraind met datapunten over monoethanolamine, 2-amino-2-methly-1-propanol en N-methyldiethanolamine. De inputs van het model zijn: de procesomstandigheden, informatie over de kolommen en de absorberende vloeistof. De output is de K_Ga_e-coëfficiënt, die de prestaties van de massaoverdracht aangeeft. Om de modellen met elkaar te vergelijken werden de R^2 score, MSE en MAE berekend voor elk model. Het ANN model kon de K_Ga_e niet accuraat voorspellen, maar toonde potentieel voor verdere verbetering. Het DTR model en SVR model met de lineaire kernel functie konden de K_Ga_e niet accuraat voorspellen, het DTR model door een gebrek aan output variantie en het SVR-lin door de niet-lineaire relatie tussen inputs en output. De SVR-modellen met de polynomiaal en radiale kernel functie voorspelde de KGae nauwkeurig en waren zeer flexibel, zowel wat betreft procesconditie, captatietechnologie, als absorberende oplossingen.

1. Introduction

1.1. CO2 emission and global warming

Global warming is the main challenge that humanity should face in the near future. In a recent summary for policymakers by the International Panel on Climate Change (IPCC) the necessity of the reduction of CO_2 emission is discussed. The panel stated that a solution to this problem is extremely urgent and needed. In open literature, it is well known how the warming went along with an increase of emission in greenhouse gasses because of the human activity. The CO_2 concentrations in the atmosphere have never been higher the last 2 million years. The rate of the warming is unprecedent over the last 2000 years. This is caused by the concentration of several gases in the atmosphere; among these, the CO_2 is the most influent. As a consequence of this warming the land temperature has risen, the arctic sea ice has reduced, the sea level rises faster, and weather and climate phenomena have become more and more signifigant across the globe [1].

The report from IPCC also reports the prediction for the next decades regarding the global warming based on the CO_2 emission. In Figure 1 and Figure 2 five possible scenarios for the future of surface temperature based on different CO_2 emission scenarios are presented. From these scenarios it can be concluded that the sooner the emission is lowered the less the rise of surface temperature will be. For this reason, the humanity requires an effective solution in the short term to this problem.

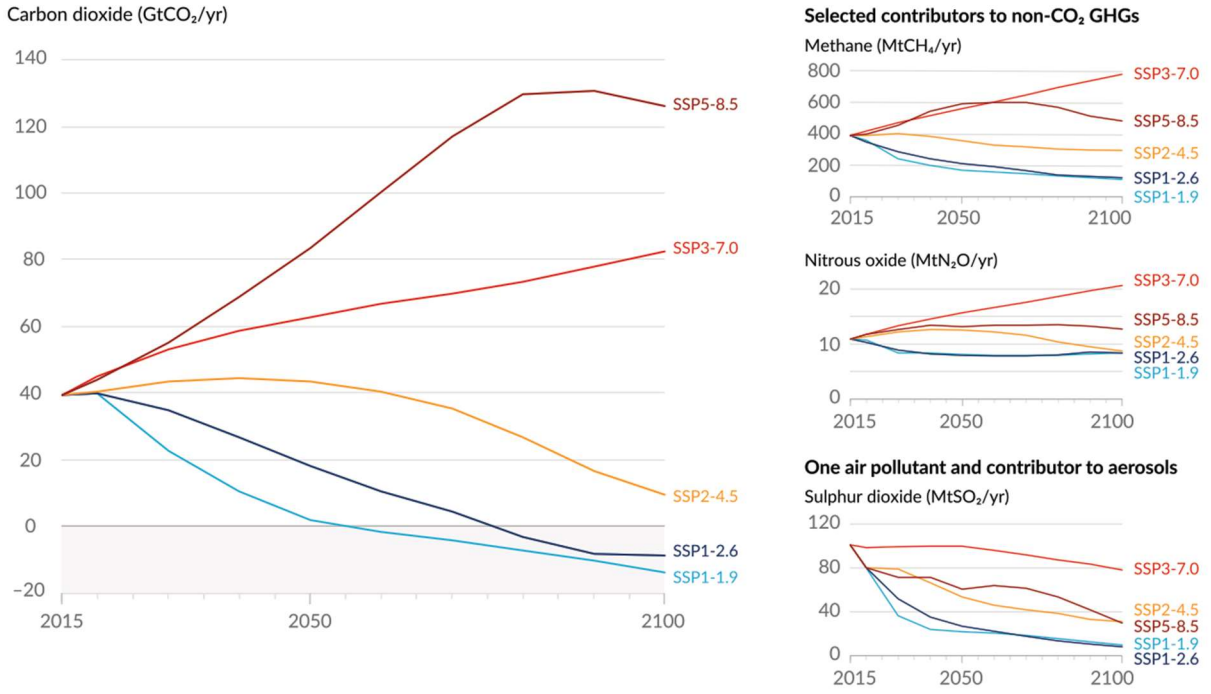

Figure 1: Future CO_2 emissions and non CO_2-drivers for five possible scenarios[1]

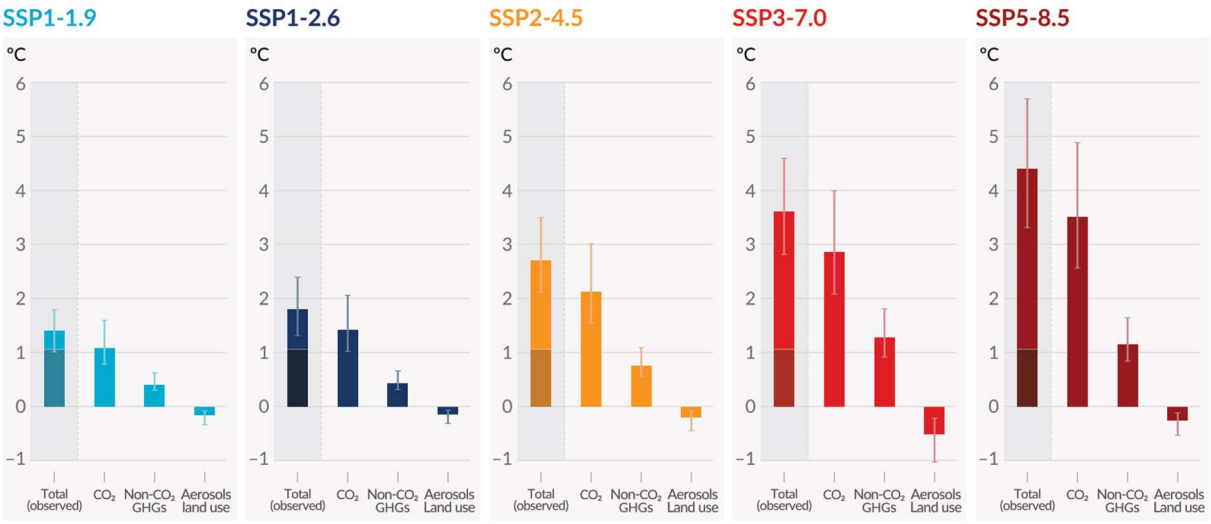

Figure 2: Contribution to global surface temperatures of the five different scenarios[1]

In the paper by Yang et al. [2] three main ways to reduce CO_2 emission are discussed. The first proposed way is to reduce the power requirement, this can be achieved by a more efficient use of the energy. The second approach is the reduction of the fossil fuels. This requires a switch to renewable energy sources and a way to stock and carry the energy, like hydrogen or batteries. The last proposal [2]is the carbon capture and storage (CCS). It is a generic term for all the technologies that focus on CO_2 capture and storage of CO_2 [2]. A report by the Benson et al. [3] discussed the potential of CCS and it concluded that CCS is a viable solution for the reduction of CO_2 emission on the short term. However, this is hindered both by the socio-economic policies and the highly cost related to the CSS process. On the other hand, CCS is the only viable option at the moment, since the transition towards green energy will take decades [3].

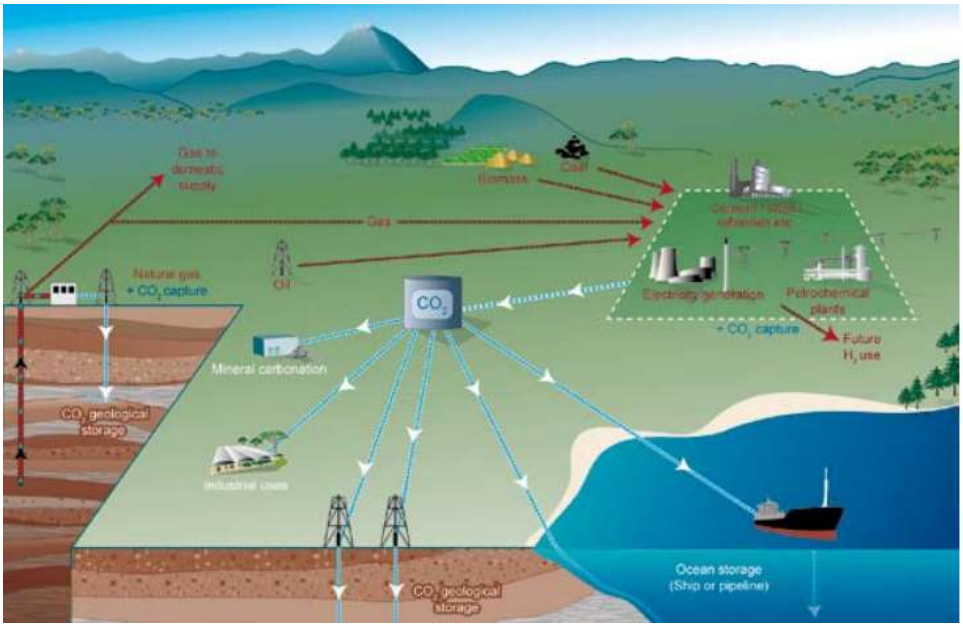

Figure 3: Different possebilities of CCS [3]

As mentioned earlier, CCS is a generic term for different carbon capture techniques. There are two main groups, namely carbon fixation and carbon separation. The carbon fixation group consists of both natural and artificial ways to directly capture CO_2. The carbon separation group contains techniques that rely on absorption and stripping processes. One of these techniques is amine absorption, this will be discussed more deeply in the next two paragraphs.

1.2. Packed bed vs spray column

The CO_2 capture process is executed in column often utilizing amine solutions. The majority of the columns employed for this process are packed columns, however in recent years spray columns are gaining attention from studies all over the world because of their enhanced transfer coefficients.

One of the first studies employing a spray column to perform carbon capture was executed by Kuntz et al. [4] It compared the mass transfer coefficients in spray and packed columns. The study concluded that the spray column has a better performances over the packed column. It was found that the spray column offers a much higher mass transfer per area tested than the packed column. The spray column needed about 75% less space to absorb the same amount of CO_2 compared the packed column. Thus that the volumetric mass-transfer coefficients factor ($K_G a_e$) value increases as the liquid flow is increased, this is opposite to what takes place in a packed column. Another side advantage of the use of spray columns is the smaller pressure drop over the column. These findings leaded to the conclusion that the CO_2 absorption column can perform at a higher absorption rate than packed columns[4].

Despite the great potential of the spray column the implementation in a large scale is minimal. This is because of the absent of an accurate model of the CO_2 capture process, that is necessary for optimisation purposes.

1.3. Different amine solutions used as solvents

The use of aqueous amine solutions for CO_2 capture is a well-established technology and is extensively used for CO_2 removal from gas streams. The amine solutions can be used both in a packed column and a spray column [4]. The most widely used aqueous amine solution is a monoethanolamine (MEA) solution [5]. However, several amine solutions that show promising potential, such as N-methyldiethanolamine (MDEA) and 2-amino-2-methyl-1-propanol (AMP) [6]–[8].

1.3.1. CO_2 capture with monoethanolamine (MEA)

MEA is one of the most used aqueous amine solutions for CO_2 capture. MEA is a primary amine with just one OH-group (Figure 4). During the absorption process, the carbamate formation is the main reaction given by equation 1 and 2. This is the preferred reaction path since the MEA carbamate that is formed is quite stable [4].

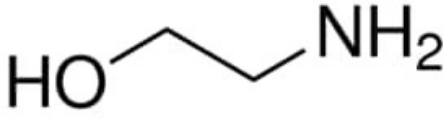

Figure 4: Structural formula of MEA

$$CO_2(I) + H_2NCH_2CH_2OH \leftrightarrow HOCH_2CH_2NH_2^+COO^- \quad (1)$$

$$HOCH_2CH_2NH_2^+COO^- + H_2NCH_2CH_2OH \leftrightarrow HOCH_2CH_2NH_2^+ + HOCH_2CH_2NHCOO^- \quad (2)$$

1.3.2. CO_2 capture with 2-amino-2-mehtyl-1-propanol (AMP)

AMP is a primary amine with one OH-group and one methyl-group (Figure 5). In the case of the AMP-CO_2 system, the carbamate formation is the main reaction. This is the same as in the MEA-CO_2 system and leads to the following reactions of equation 3 and 4:

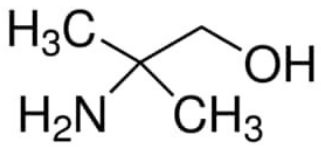

Figure 5: Structural formula of AMP

$$CO_2(I) + H_2NCH_2OH \leftrightarrow HOCH_2C(CH_3)_2NH_2^+COO^- \text{ (3)}$$

$$HOCH_2C(CH_3)_2NH_2^+COO^- + H_2NC(CH_3)_2CH_2OH \leftrightarrow HOCH_2C(CH_3)_2NH_2^+ + HOCH_2C(CH_3)_2NHCOO^- \text{ (4)}$$

The carbamate that is formed will start to form a hard soluble salt, unlike the carbamate that is formed in the MEA-CO_2 system.

1.3.3. CO_2 capture with N-methyldiethanolamine (MDEA)

MDEA is a tertiary alkanol amine. In Figure 6 the structural formula of MDEA is shown. Because MDEA is a tertiary amine it has a higher stoichiometric CO_2 loading than MEA and AMP, but the reaction speed is slower. This is related to the different reaction mechanism for the absorption of CO_2 compared to the primary and secondary amines. The tertiary amine does not react directly with the CO_2, but it acts as a base, and so catalyzing the hydration of CO_2 [7]. This leads to the following reaction given by equation 5:

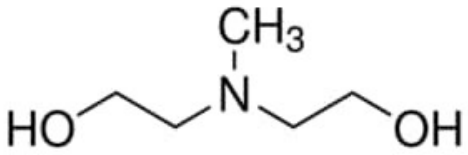

Figure 6: Structural formula of MDEA

$$CO_2 + R_1R_2R_3N + H_2O \leftrightarrow R_1R_2R_3NH^+ + HCO_3^- \text{ (5)}$$

1.4. State of the art first-principle models

First-principle models use thermodynamic laws, reaction kinetics and balances to model a chemical process. These models rely heavily on theoretical evaluations and the previous knowledge about the studied process [9]. They are currently used to predict the behavior of the CO_2 absorption in columns. In a study by Q. Zang et al. [10] a rigorous rate-based model employing Murphree efficiencies in the column and rigorous pressure drop calculation methods provided a steady-state model. This model gave accurate results, but it is very complicated and requires long modelling times. A simpler rate-based model was created by Razi N. et al. [11] and the modelling times were shorter, but the model could not predict all the uncertainties of the process and was therefore not representative.

These first-principle models were all used to predict the CO_2 absorption in a packed column, however they fail when applied to a spray column. This is because a spray column has higher intercorrelations of variables, which makes it difficult to isolate the various effects. A first-principle model created by Yin Xu et al. [12] was able to predict the CO_2 absorption in a spray column, however it had a deviation of 15%. This shows that despite the high number of intercorrelations between variables that were included the model could still not accurately predict the CO_2 absorption.

It can be concluded that the first principle models come with a tradeoff between accuracy and computational times. However, this tradeoff is not the only weakness of a first-principle model. In order to model the CO_2 capture both the phenomena taking place and a model of these phenomena needs to be known. This is not the case for CO_2 capture in spray; therefore to increase the accuracy of the model a machine learning (ML) solution is needed.

1.5. Machine learning applications in chemical industry

Machine learning is branch of computational algorithms that is designed to emulate human intelligence by learning from a surrounding environment. The algorithm learns from the input data to produce a desired output, this without any programmed logic behind it [13]. Machine learning has many applications: computer vision, prediction, semantic analysis, natural language processing and information retrieval [14]. In this thesis the prediction application will be used.

In chemical industry machine learning is an established technique since the 1980's, however due to the lack of computational power the applications were limited. In the last decades the computational capabilities increased. This let the machine learning techniques be more and more used in chemical industry. Machine learning is one of many artificial intelligence (AI) techniques and it is defined by Dobbelaere M. et al. as a subset of AI including all techniques that enable computers to learn from experience [15]. A machine learning model can be divided in three main components: data, representation of the data and the model itself. The data is important because it is used to train and validate the created the model. The quality of the data is a crucial factor, because if the data do not accurately represent the physical world the model will learn a false trend. The quantity however is equally important, since the model is than able to distinguish outliers from the dataset. The representation of the data is second important component, it is crucial to select the most significant features of the dataset to keep the number of features low. This will reduce the computational time required for the training of the model while increasing its the accuracy. The model itself is the last important component of machine learning, there are many different kinds of machine learning models, all of which can be divided into two main classes: unsupervised learning and supervised learning [15]. In Figure 7 the two main classes are shown with examples of machine learning models.

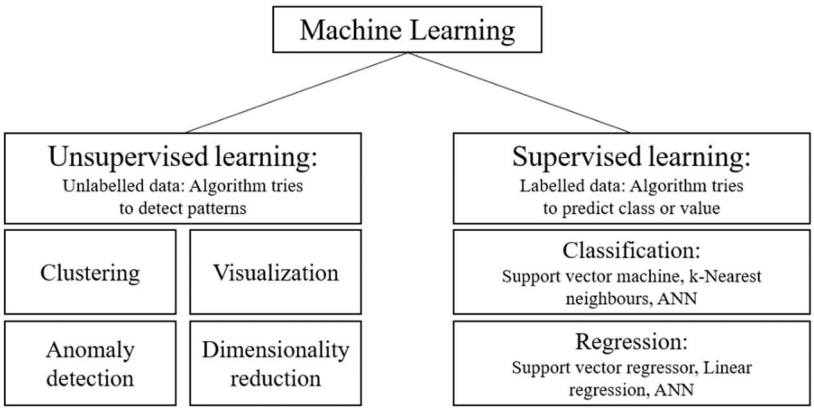

Figure 7: Overview of different types of machine learning

In the unsupervised learning the training is not executed on the classical input-output relation but it is used to detect the underlying structure of the data. In the supervised learning the training is executed on a dataset containing both the input and the output of the observed system. This creates a model that correlates these two values. This approach is often used to model chemical processes or to monitor the online quality of a process.

In this master thesis the supervised learning models will be used, namely a support vector regressor, artificial neural network and a decision tree regressor.

As the use of machine learning in chemical industry will increase in the future, different challenges and opportunities will arise. Both Dobbelaere et al. [15] and Schweidtmann et al. [16] identified the following six challenges and opportunities. Optimal decision making, introducing and enforcing physics in ML, information and knowledge representation, heterogeneity of data, safety and trust in ML applications, and creativity.

1.6. Different kinds of supervised machine learning algorithms

As mentioned in paragraph 1.4 a first principle model is not able to accurately describe the process of carbon capture in a spray column. However, machine learning algorithms can provide a solution [9], [17]. Machine learning algorithms create a model utilizing the data to develop its internal structure. The model approximates the functional relationships between the input and the output of the observed system. These relationships obtained from the experimental data will be represented in the model during the training phase. Therefore, a machine learning algorithm approximates only on the relationships between input and output data without relying on thermodynamic principles, reaction kinetics and first-principle information. On the other hand, this can represent a weakness for the machine learning applications when the dataset contains noisy or wrong data or does not cover the entire experimental space. For this reason, the quantity and the quality of the data are a crucial parameter to model this process. It is important to feed only a selection of features of the dataset to the model. To determine which input parameters are the most important least-squares-based algorithms are often used [17]. The different kinds of machine learning algorithms used in this master thesis will be discussed next.

1.6.1. Artificial neural network (ANN)

One of the machine learning algorithms used to create a model in this work is an artificial neural network (ANN). The base element of a neural network is the artificial neuron. Its structure is shown in Figure 8. Each neuron takes a certain amount of input (x_i) and returns one output (y). It is divided in two parts: the linear part and the activation function. In the linear correlation step each input of the neuron is multiplied by a weight (w_i), these factors are then summed ($\sum x_i w_i$), and a bias is given. Then the result of the linear operation is utilized as input of an activation function $f(\sum x_i w_i)$, that add non-linearity to output of the neuron. The tunable parameters of the artificial neurons are the weights and the bias in the linear correlation.

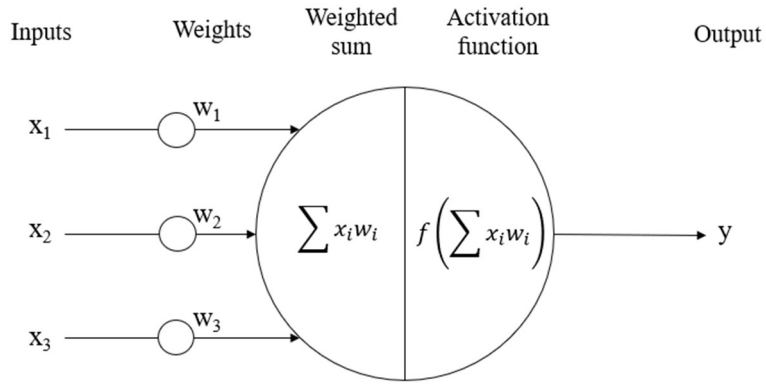

Figure 8: Structure of an artificial neural network

In a neural network, the neurons are organized by layers. Each layer takes input from the layer behind him and give its output to the next layer. An example of an ANN structure with one hidden layer is shown in Figure 9.

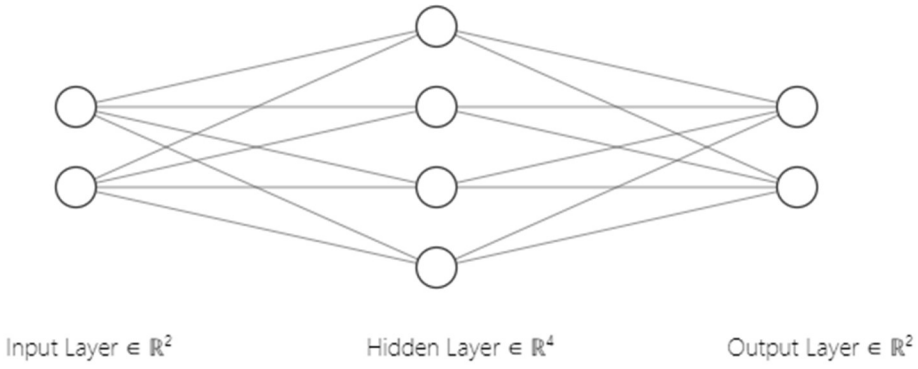

Figure 9: Structure of an artificial neural network

The information fed to the input nodes are the input values of the model, each neuron represents one input parameter. The neurons in the hidden layer and the output layer get their input information from each neuron of the previous layer. The result coming from the output layer consists of the modelled output variable. This type of network architecture is called a multilayer perceptron.

During the training phase of the network, the obtained information from the dataset is stored in the weights and the bias of each neuron. This learning algorithm is based on a cost or error function, this function measures the difference between the modelled output and the actual output [9].

The mean squared error function (MSE) is often used as a cost function and is given by equation 6 [9]:

$$MSE = \frac{1}{N} * \sum_{i=1}^{N} (y_i - \hat{y}_i)^2 \ (6)$$

where n is the number of samples used for the evaluation, y_i is the experimental value of the i-th sample of the dataset and $\hat{y}_1$ is the predicted value for the i-th sample of the dataset. The goal of the training and the cost function is to minimize the MSE and thus finding the optimal configuration for the network.

The main advantage of an ANN is the possibility to accurately model complex problems with a highly modular structure. It is also able to handle many input parameters and, once it is trained, it is easy to use and require low computational time [18]. All these benefits are because of four basic characteristics of an ANN. It is non-linear, the artificial neurons mimic this behavior in the mathematical performance of a non-linear relationship. It is non-limited, because the neural network consists of multiple neurons not only the neurons themselves determine the behavior of the network but also the relationships between the different neurons. It is non-qualitative, this means that it has self-adaptive, self-organizing, and self-learning ability. The fourth characteristic is the non-convexity, which means that the function has multiple extrema, thus the system has multiple stable equilibrium states.[19].

Despite all these promising characteristics of an ANN it also has some significant drawbacks that cannot be denied. The first problem is the robustness of the ANN models because the capability of an ANN model depends on the general trend of the training dataset. In other words, the accuracy of the ANN model highly depends on the accuracy of the dataset. A second limitation of an ANN model is it transparency and the lack of knowledge extraction from it. It is quite hard to interpret the relations between the input and output used by the ANN. Furthermore, an ANN also has a poor extrapolation capability, the model accuracy is poor outward the range of the training dataset. The final problem of an ANN is its limitation in including uncertainties in its predictions. This makes it difficult to judge the quality of an ANN prediction [18].

Despite these problems the use of ANN models over the past decades increased. In engineering and industry applications ANN models are mostly used for making predictions and for pattern recognition in data [18]. The same is true for CO_2 capture, multiple ANN models have been developed to predict different CO_2 capture processes [9], [20]–[25]. The same modelling is also successfully applied in the SO_x absorption. All these studies concluded that an ANN model has great potential to model CO_2 processes and the ANN models were more accurate compared to the first principle models.

The objective of the ANN created in this research is to predict the $K_G a_e$ value of the CO_2 capture in the spray columns.

1.6.2. Support vector machine (SVM)

A support vector machine (SVM) is a supervised learning modelling technique. Often it is used for classification tasks, but it can also be used for regression tasks. In this thesis the SVM is used for regression purposes and therefore it is called a support vector regressor (SVR).

In Figure 10 the four main parts of a SVR are shown: the kernel function, the regressor, the maximum error and the soft margin. First the kernel function maps the input dataset into a higher dimension space. Once all the input data is mapped the regressor fits the mapped data points. In contrary to ordinary regression models the goal of the training of the SVR is not to minimize its errors. Instead, the aim is to minimize the loss function, the l2 norm of the coefficient vector. The error of the SVR is handled a different way, namely it is constraint where the absolute error is given by a margin being the maximum error (ε). By tuning ε the desired accuracy can be gained. However, it is possible that a datapoint is not constraint by the maximum error. This is done using a slack variable, namely the soft margin (ξ) which is the deviation between the maximum error and the value of the data point. This soft margin is also included in the loss function, because it is desirable to minimize it.

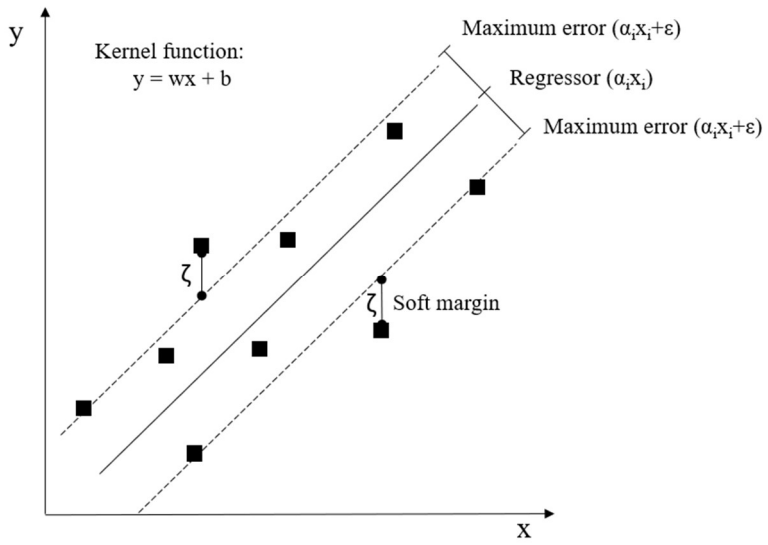

Figure 10: Working principle of a support vector machine

A SVR is much more robust than an ANN, this is due to the difference in training ways, which means that a SVR has a better generalization and training efficiency. Because a SVR uses a kernel function to map the input data it is easier and more efficient to analyze the input data, in comparison to an ANN. The last strength of a SVR is its error-complexity, unlike a ANN, which uses mean squared errors to suppress outliers in the dataset, a SVR uses a soft margin and maximum hyperplane. Because both parameters are tunable, a SVR is more robust to the outliers than an ANN. However, this directly leads to one of the main weaknesses of an SVR. In order to have an accurate training of the SVR, the hyperparameters selection (i.e. soft margin dimensions and kernel functions) is a crucial operation.

This can be a hard task which requires some experience and time. In addition, for large training datasets it can take a lot of time to find the most optimal value for the main four parts of a SVR [27].

SVR are used for multiple implementations in chemical industry, it is used to design drugs in the pharmaceutical industry [28] or to estimate performance of chemical plants [29] or as a risk assessment [30]. But in comparison to ANNs, SVR are less used for modelling CO_2 capture. However not much research is done on this application, which means that its true potential is still unknown. In this master's thesis the goal of the SVR model is the same as for the ANN model.

1.6.3. Decision tree regressor (DTR)

The decision tree regressor (DTR) is a model which learn from datasets to preform regression problems. The DTR consists of three main parts: root, discission nodes and leaf nodes (Figure 11).

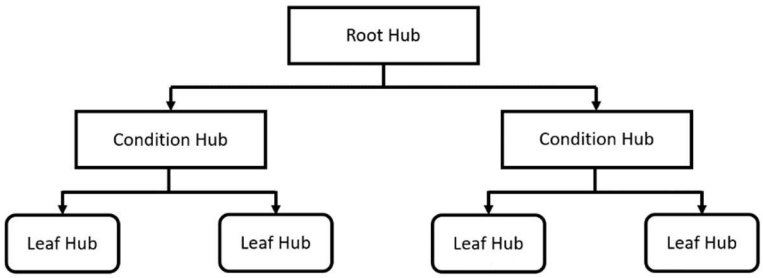

Figure 11: Structure of a decision tree

The first important part of the decision tree is the root hub, here the dataset is split into two based on whether a certain condition was met. Afterwards the two sides are split again into two sides based on another condition. This splitting goes until the datasets can no longer be split into two or when the maximum splitting amount is met or when the splitting does not influence anymore the overall error prediction. When one side is no longer split in two a leaf hub is created. This represents the output of the model.

To create the optimal structure for the decision tree, the root hub and condition hubs have to be determined. First each input feature is plotted versus the output feature, and for each input feature all the possible splits are made. For each side of the split the average output value is calculated. Then the sum of squared residuals between the output of each data point and the average of the split is made. The sum of squared residuals is given by equation 7:

$$sum\ of\ squared\ residuals = \sum(y_{avg} - y_i)^2 (7)$$

Then for each input feature the split with the lowest sum of squared residuals is chosen as the condition hub for that input feature. Following, the decision tree is built from the top down, with the root hub being the condition hub with lowest sum of squared residuals and the following condition hub being the one with the second lowest sum of squared residuals. The number of condition hubs is determined by the max depth of the tree or by the minimum split condition. The max depth of the DTR gives the maximum number of layers the DTR and the minimum split condition gives the minimum number of data points that a branch must have in order to have a condition hub.

Once a branch can no longer be split it becomes a leaf hub, which means that all the data point that fulfil to the condition of this leaf hub will get the average output of the train dataset that fulfil this condition.

Like the ANN and the SVR, the DTR modelling technique has some strength and weaknesses in its application. The first main strength of the DTR is the higher possibility to explain the decision path to generate the output compared to an ANN network. This is allowed by the "what-if" structure that the DTR develops that can be easily read and understood. This makes it ideal for data exploration because it is a fast way to generate relations in your data. The second main strength of the DTR is its training time since it has less tunable parameters compared to the ANN and SVR. The only tunable parameters of the DTR are the maximum depth that the tree can reach and the split condition, this takes less time to tune than the parameters of an SVM. However, these strength also lead to the main weakness, namely overfitting. A DTR has a sensitivity for overfitting, especially for large datasets with a lot of features, which can lead to higher error prediction compared to the ANN and SVR.

The DTR has multiple implementations in chemical industry, it is used to model the solubility of CO_2-N_2 gas mixtures [31] or to model data from soft sensing parameters [16] or to predict the material removal rate for chemical mechanical planarization [32]. The DTR has also been used for modelling CO_2 absorption in amines [33], [34].

2. Materials and methods

In this chapter the materials and methods used in this master's thesis are discussed. The thesis focuses on modelling the CO_2 capture using amine solutions. To train the models a dataset is needed, however there is not enough literature data available on AMP solutions. For this reason, an experimental work was added to the thesis. It focused on the collection of data about the performance of AMP solution in CO_2 capture process. Following, the data collected in the experimental work of this thesis were integrated with data from literature and five different models were trained to predict the $K_G a_e$ coefficient of the column.

2.1. Experimental data collection

In this paragraph is explained the experimental set-up utilized to collected part of the training data.

2.1.1. Solution preparation

For the experiments two different amines were used, namely monoethanolamine (MEA) and 2-amino-2-methyl-1-propanol (AMP). The MEA had a purity of higher than 98% and the AMP had a purity of 90%, both were purchased from Sigma-Aldrich. The aim of the experimental part is to investigate how these two amines behave when utilized for the carbon capture. In Table 1 the compositions of the five prepared amine solutions are shown.

Table 1: Composition of amine solutions

%wt AMP	%wt MEA	Name
100	0	100AMP0MEA
70	30	70AMP30MEA
50	50	50AMP50MEA
30	70	30AMP70MEA
0	100	0AMP100MEA

Then to further investigate the system water was added to each of these mixture to create solutions with the 30, 50, 70, 90 and 100 amine %wt in water.

The solutions were prepared using a semi-automatic balance and demineralised water was used to dilute to the right amine %wt. To ensure the homogeneity of the prepared solutions, a magnetic stirrer was used for 10-15 minutes before the solution was used in the experimental set-up.

2.1.2. Experimental set-up

The experimental set-up that was used in this master's thesis is a spray reactor for carbon capture, the set-up is shown in Figure 12.

Figure 12: Experimental set-up for carbon capture

The set-up has two main gas supplies, namely a N_2 gas supply (1) with a separate pressure regulator (2) and a CO_2 tank with a pressure regulator (3). For the low gas flow rates a Bronkhorst EL-FLOW Select MFC (4) is used, which goes up to 2 L/min for CO_2 and 3 L/min for N_2. For the higher gas flow rates a Bronkhorst EL-FLOW Prestige MFC (5) is used, which goes up to 80 L/min for CO_2 and 100 L/min for N_2. All mass flow controllers are calibrated at a temperature of 21°C and at an inlet pressure of the gas at 3 bar, except for the low N_2 mass flow controller which is calibrated at 5 bar. The use of 4 different flow controllers allows a fixed inlet CO_2 %vol for every gas flow rate within the range of the flow controllers. After the CO_2 and N_2 leave the flow controllers they are mixed in a T-junction and then send to the reactor (11).

The amine solution (6), is pumped from its container by a KNF SIMDOS 10 FEM 1.10S (7). After passing through the pump the amine solutions go through a pulsation damper (8), to ensure a constant flow rate through the ultrasonic nebulizer. This ultrasonic nebulizer is an UP200St ultrasonic processor (9) and a S26d18S sonotrode (10) (Hielscher Ultrasonic GmbH) made of titanium. The ultrasonic nebulizer uses ultrasound to create a spray of nebulised amine-solution. The ultrasonic nebulizer tip is placed within the reactor. For this reason, the amine solution enters into the reactor as nebulized spray.

Inside the reactor the carbon capture process takes place. The reactor is in glass, and it has two different rooms. The inner room, where the carbon capture takes place, has a volume of 56 ml. The outer room serves as a cooling jacket and has one inlet and one outlet for the cooling water, for which tap water is used. The cooling is needed to remove the heat of the reaction and keep the reactor a constant temperature of around 24°C. The temperature inside the inner room of the reactor is measured by a DS18B20 Digital temperature sensor connected to an Arduino. The gas mixture and the amine-solution leaves the reactor and enters into a liquid-gas separator (12). The liquid phase, represented by the amine solution, leaves the set-up through a tap at the bottom of the separator. The gas mixture leaves at the top right of the separator and passes first trough a safety valve which opens at 0.5 bar. After the safety valve the gas mixture passes through a glass silica dryer (13) to filter out the water and the amine left in the gas. The silica dryer is filled with silica gel granulates with a diameter of 1-3 mm from Merck. The silica dryer protects the O_2 and CO_2 sensors which are placed after it. The O_2 sensor is connected to the Arduino and is used to measure the O_2 concentration, because spraying amine-solutions in the presence of oxygen can lead to an explosion. The CO_2 sensor (14) is a ExplorIR®-M-100 from Angst+Pfister Sensors and Power, Germany. The CO_2 sensor measures the outlet CO_2 %vol, hence the gas mixture is passed through the CO_2 sensor it is released into the fume hood.

2.1.3. Experimental procedure

At first, both gas tanks are opened and both pressure regulators are set to their correct pressure according to which flow rate is to be used. Then the PC is started and connected to the right flow controller. On the PC the programs FlowDDE and FlowView are opened and the desired flow rates for CO_2 and N_2 are set. Afterwards the set-up needs to be purged with CO_2 and N_2, this to ensure there is no O_2 left in the set-up. As mentioned earlier spraying amine-solutions in the presence of O_2 can lead to dangerous scenarios. The amount of O_2 can be read from the serial monitor of the Arduino, which is connected to the O_2 sensor. While the O_2 is purged out, the set-up can be checked for gas leaks using foam.

Once all the set-up is purged and leak-proof the set-up can be used. First the inlet %vol of CO_2 is read by using the GSS program on the PC. Once the CO_2 %vol is stable on the desired level it is recorded using the GSS program. After one minute of recording the ultrasonic nozzle and the pump of the amine-solution are started. After a while the CO_2 %vol will reach a stable level again and it can be concluded that the carbon capture process is complete. The recording is now stopped, and the pump and ultrasonic nozzle are both turned off.

When the amine-solution is changed or at the end of each day, the set-up is thoroughly rinsed with water to remove all the residues of amine solutions into the reactor.

2.1.4. Experimental plan

The first part of experiments consisted of screening experiments, because AMP was never tested on this set-up before the optimal operating conditions were not known.

The screening experiments had two different goals: 1) determining which AMP-solution preformed best and 2) investigate the best range of operating conditions. The operating conditions that were changed are: liquid flow rate, gas flow rate, CO_2 %vol and $nAmine/nCO_2$. Four different AMP solutions were used: pure AMP, AMP-water, AMP-MEA and AMP-MEA-water. All these solutions were tested for different AMP %wt.

From the screening experiments it was concluded that the AMP-MEA-water solution was the most promising out of the four tested solutions. An experimental plan was drawn to research the influence of AMP/MEA ratio, the water %wt, nAmine/nCO_2 and CO_2 %vol. In total 70 experiments were executed and the operating conditions and results of the screening experiments can be find in the appendix A.1.

2.1.5. K_Ga_e coefficient

In order to evaluate the performances of the CO_2 capture process, the K_Ga_e coefficient for each experiment is calculated. The K_Ga_e coefficient includes three aspects of mass transfer in a CO_2 absorption system. These are the thermodynamics of the system, the kinetics of the system and the hydrodynamic nature of the absorption equipment [4]. The K_Ga_e can be calculated using the equation 8:

$$K_G a_e = \left(\frac{G_I}{P\left(y_{CO_2} - y^*_{CO_2}\right)}\right) * \left(\frac{dy_{CO_2}}{dh}\right) \quad (8)$$

Where K_Ga_e is the overall mass transfer coefficient (kmol.m^{-3}.kPa^{-1}.h^{-1}), G_I is the inert gas molar flux (kmol.m^3.h^{-1}), P is the total system pressure (kPa), y_{CO2} is the molar fraction of CO_2 in gas bulk, y^*_{CO2} is the molar fraction of CO_2 in equilibrium with liquid and bulk concentration and h is the height of the absorption zone (m). The K_Ga_e coefficient can be used to compare the performance of different amines and different operating conditions. In this research, the K_Ga_e coefficient is the parameter that will be modelled.

2.2. Modelling approaches description

2.2.1. Data collection

The data used to train all the models in this work were obtained from four different sources. The first set of data are the points collected during the experimental part of this thesis. As mentioned in paragraph 2.1.1., six different AMP-MEA mixtures were used in a spray column set-up. A second set of data were obtained utilizing pure MEA and MEA-water to run the absorption test. These were collected by A. Van den Bogaert [35] on the same set-up as the one used in this thesis. The data set was than further enriched by 2 datasets from literature. One dataset consisted of MDEA, MEA and MDEA mixtures, that were tested pure and diluted with water, the points were all collected in a packed column with Sulzer DX packing [36]. The other literature dataset consisted of AMP-MEA data, that was diluted with water, the points were all collected in a packed column with Sulzer DW packing [37]. In Figure 13 the distribution of the dataset is shown.

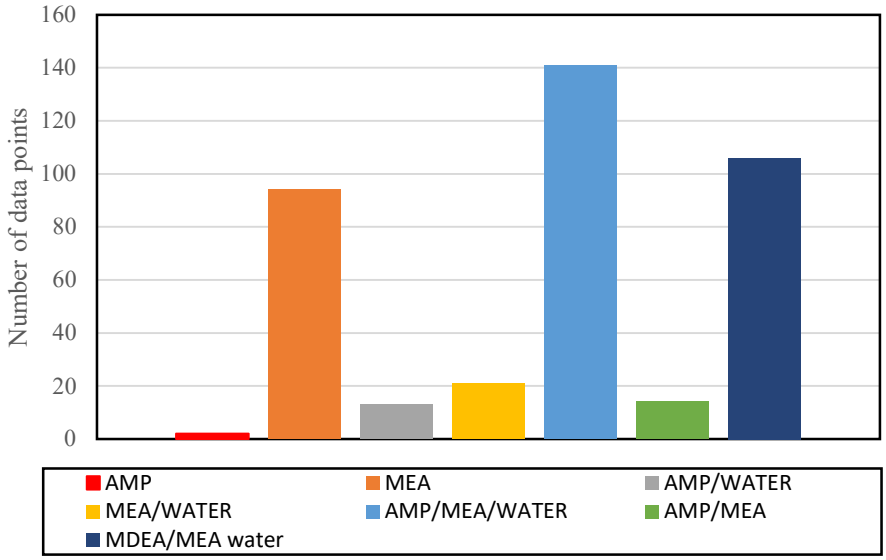

Figure 13: Distribution of the dataset

2.2.2. Feature extraction and preprocessing

The input features of the ML models were the same among the various models and can be divided in three categories. Namely, the input parameters of the set-up, composition of the amine solutions and chemical properties of the amines. The input parameters of the set-up are: CO_2 %vol, total gas flow rate, liquid flow rate, nAmine/nCO_2 and the interfacial area of the column. The interfacial area between the gas and the liquid was included, in this way the model can be used both in spray and packed columns. The composition of the amine solution is reported as the weight percentages of all the amines. The chemical properties utilized as input of the model are the density, the dynamic viscosity, kinematic viscosity, surface tension and the diffusion coefficient. Further information about these properties can be found in appendix A.2.

To facilitate the model training, the data are processed, namely a normalization in the range [0,1] or a standardization are applied depending to the utilized model. This operation is executed utilizing the function MinMaxScaler and StandardScaler implemented in the library scikit-learn 0.23.2 [38]. In addition, to evaluate the generalization performances of the model, the validation dataset was divided into train and validation set. The train set was the only one utilized during the training phase, while the validation set was used to assess the generalization capabilities of the model.

The MinMaxScaler is used to scale the input features for the artificial neural network. The MinMaxScaler scales all the input data to a value between 0 and 1 and uses equation 9 [38]:

$$x_{std} = \frac{(x - x_{min})}{(x_{max} - x_{min})} \quad (9)$$

Where x_{std} is the normalized value of the input, x_{min} is the minimum of the feature input, x_{max} the maximum of the feature input, x is the value of the data point.

The standard scaler is used to scale the input features of both the support vector regressors and the decision tree regressor. The standard scaler standardizes each feature by removing the mean and scale to unit variance. This allows for a more sufficient training of the SVR and DTR model. Equation 10 is used to standardize each feature:

$$z = \frac{x-u}{s} (10)$$

Where z is the standardized input value, x is the non-standardized value of the input point, u is the mean of the feature samples and s is the standard deviation of the feature sample. This means that the mean of the standardized values is 0 and the standard deviation is 1, which leads to a normally distributed dataset.

2.2.3. Artificial neural network

The ANN used in this thesis is a multilayer feed-forward network, which employs a back-propagating learning process. The ANN was implemented using the Pytorch 1.11.0 [39]. The optimized structure was obtained by tuning all the hyperparameters of the ANN with an empirical trial and error method. The most optimal network was determined by the MSE of the test dataset. The structure of the finale model is shown in Table 2.

Table 2: Structure of the ANN model

Layer	Number of nodes
Input layer	17
Hidden layer 1	30
Hidden layer 2	15
Hidden layer 3	30
Hidden layer 4	15
Hidden layer 5	30
Hidden layer 6	15
Output layer	1

Likewise, also the optimal activation functions were also obtained using a trial and error method, which used the MSE of the test dataset as score. For the input layer and the hidden layers a Rectified Linear Unit (ReLU) activation function was used. The ReLU activation function is given by equation 11.

$$y = max\ (0, x) (11)$$

Where y is the output, x is the input given to the ReLU function.

The output layer has a different activation function than the internal layers, namely a hyperbolic tangent (Tanh) activation function. The Tanh activation function is shown in equation 12.

$$y = \frac{e^x - e^{-x}}{e^x + e^{-x}} (102)$$

Where y is the output and x is the input data point.

Because of the size of the network, it was observed that the back-propagation algorithm results is highly influenced by the initial guess of the weight. It was observed that the Xavier Uniform distribution gave the lowest MSE and the most repeatable results among the various training [40].

[40]The optimization algorithm utilized for the training of the network was the AdamW. The goal of the optimizer and training is to minimize the loss function, in this thesis the MSE is used as loss function and is given by equation 6. The MSE is calculated between the modelled $K_G a_e$ and the experimental $K_G a_e$ on the validation dataset. The training follows a backpropagation, it starts by tuning the weights and biases of the neurons between the output

layer and the last hidden layer. Afterwards it moves to the next layer of neurons until all neurons are tuned. This training sequence is repeated a specific number of times, which is specified by the number of epochs. In this thesis 450 number epochs were used.

2.2.4. Support vector regressor

In total three different support vector regressors (SVR) were trained in this thesis. Each SVR had a different kernel function. The general estimation function of the SVR is given by equation 13.

$$y = \sum_{i=1}^{n} \alpha_i * K(x_i, x_j) + b \quad (13)$$

Where y is the output of the model, α_i are the support vectors, $K(x_i,x_j)$ is the kernel function, b is the bias.

As mentioned above, three different kernel functions were used in this thesis: polynomial function (equation 14), linear function (equation 15) and radial basis function (equation 16).

Polynomial kernel function:

$$K(x_i, x_j) = (x_i * x_j + r)^d (14)$$

Where x_i and x_j are the values of different data points, r is a constant and d is the degree of the polynomial.

Linear kernel function:

$$K(x_i, x_j) = (x_i - x_j + r) (15)$$

Where x_i and x_j are the values of different data points and r is a constant.

Radial basis kernel function:

$$K(x_i, x_j) = e^{-\gamma(x_i - x_j)^2} (16)$$

Where x_i and x_j are the values of different data point and γ is the scaler.

The goal of the training phase of the SVR to minimize the loss function expressed in equation 17, by tuning the values of α_i, c and ξ_i.

$$min(\frac{1}{2}(|\alpha_i|)^2 + c \sum_{i=1}^{n} |\xi_i|) \quad (17)$$

Where α_i is the support vector, c the regularization parameter and ξ is the soft margin. The regularization parameter determines how tolerant the soft margin is and is a tunable parameter.

However the training, is constrained, this means that the values of α_i, c and ξ_i must comply with the constrain given by equation 18 and cannot have any value that give the minimum of equation 17.

$$|x_j - \alpha_i x_i| \leq \varepsilon + |\xi_i| (18)$$

Where ε is the maximum allowed error.

To find the most optimal SVR model the hyperparameters are tuned using a gridsearch. The gridsearch contained the following hyperparameters: regularization parameter (c), degree (d)

and maximum error (ε). During the gridsearch of the model a cross-validation was used in order to ensure the robustness of the model on unseen data [41]. In this thesis the training dataset was split into 10 for the cross-validation. The cross validation means that the dataset is split into 10 equal pieces. In turn, each piece is chosen as validation set of the network and the rest is selected to compose the training set. In this way the accuracy of the model on the validation set can be estimated and the hyperparameter selection is more effective. But it also means that the model will be trained 10 times using the same set of hyperparameters. The score of the training is based on the R^2 score of the modelled results from the validation dataset. The goal of the training is to tune the support vectors (α_i) and the bias (b) to minimize equation 17. In Table 3 the best hyperparameters of the three SVR models created in this thesis are shown.

Table 3: Hyperparameters of the SVR models

Model name	C	Degree	Epsilon	Kernel function
SVR-poly	50	3	0.05	Polynomial
SVR-lin	40	1	0.3	Linear
SVR-rbf	50	1	0.01	Radial based function

2.2.5. Decision tree regressor

In this thesis one model using a decision tree regressor was created. The hyperparameters of the model are the max depth of the decision tree and the min sample split condition. The hyperparameter of the model were tuned by using a gridsearch with a 10-fold cross validation. The most optimal parameters are shown in Table 4.

Table 4: Hyperparameters of the DTR model

Max depth	7
Min sample split	0.1

3. Results and discussion

In this chapter, the results from this master's thesis are discussed. The thesis includes an experimental part, where the training data for the models is collected. The results of these experiments will be discussed first, afterwards the performance of the different models will be discussed.

3.1. Experimental results

3.1.1. Screening results

The first set of experiments executed in this work aimed to screen the experimental space. The aim of this initial screening phase was to perform a physical based design of experiments. The results were used as training data for the models and can be found in the appendix A.1. of this work. Since these were screening experiments, the results will not be discussed in detail, but two main conclusions can be drawn:

1) At higher CO_2 loadings and high AMP concentration, there is a salt formation that let the viscosity of the liquid increase. This salt was observed to be soluble in the water. Because the salt formation caused the set-up to clog, it is desirable to keep the AMP/water ratio below 7. These findings are based on visual observations and are in line with what F. Barzagli et al. [42] reported. The salt formation was not further investigated in this work, because this falls outside the research topic of this master's thesis.
2) AMP/MEA solutions had a higher overall K_Ga_e than the AMP/water solutions. For the DOE an AMP/MEA/water was used, although the K_Ga_e of AMP/MEA was the highest water was added to make sure the set-up did not clog.

3.1.2. Effect of water concentration and AMP/MEA ratio for nAmine/nCO_2 = 2

The effect of water concentration and AMP/MEA ratio for nAmine/nCO_2 = 2 the K_Ga_e value and the absorption efficiency are shown in Figure 14 and Figure 15. The nAmine/nCO_2 was set at the stoichiometric value of 2 and CO_2 concentration was set at 10%vol.

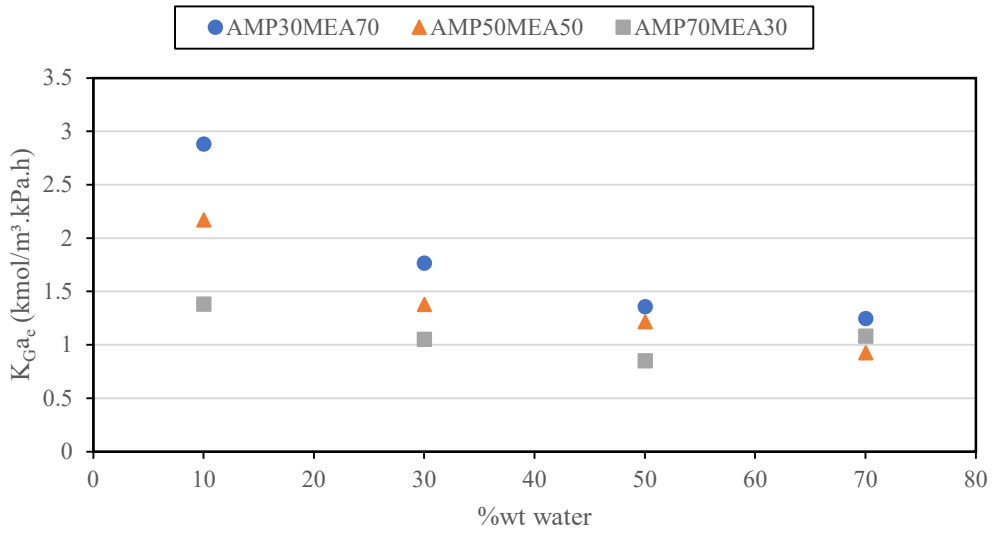

Figure 14: Effect of water %wt and AMP/MEA ratio on K_Ga_e for nAmine/nCO_2 = 2

For the datasets where MEA is the prominent amine (i.e. AMP30MEA70 and AMP50MEA50) the K_Ga_e value decreases with the amount of MEA. This is expected because the overall reaction speed of MEA is higher than those of AMP and water. Since K_Ga_e is a coefficient to express the mass transfer, it is logical that pure MEA has the highest K_Ga_e, because of the higher overall reaction rate [43]. The same trend however does not occur in the AMP70MEA30 dataset, here AMP is the prominent amine. In this case the K_Ga_e value at first decreases then rises again when the water concentration goes from 50%wt to 70%wt. This is most probably the effect of the salt formation which occurs during the reaction of AMP with CO_2. The formed salt is soluble in water and thus the higher is the water concentration in the solution the higher is the solubility of the salt. Therefore, the equilibrium of the reaction is changed, this results in more captured CO_2.

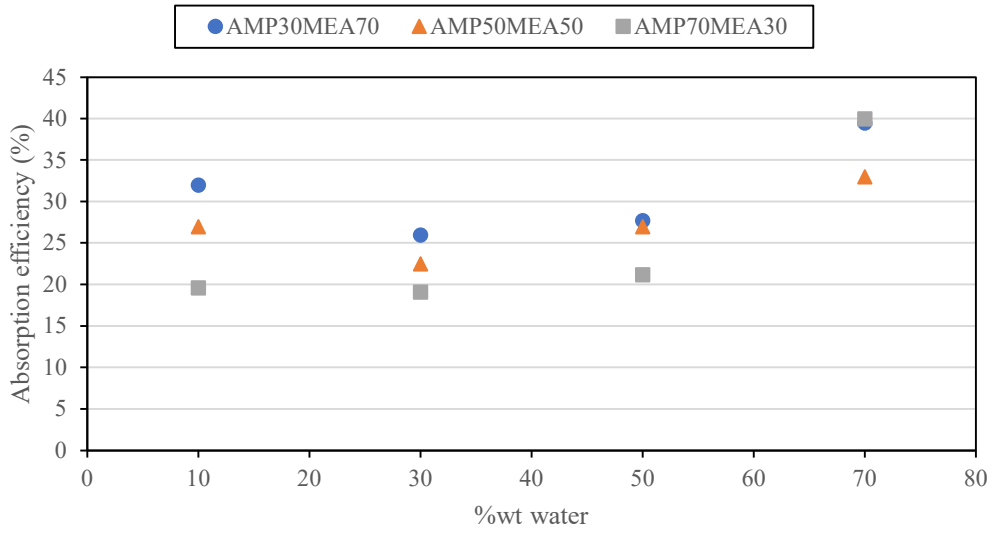

Figure 15: Effect of water %wt and AMP/MEA ratio on absorption efficiency for nAmine/nCO_2 = 2

The trend of the absorption efficiency with the water concentration in Figure 15 differs depending on the AMP concentration in the absorbent solution. In all the datasets the absorption efficiency decreases when the water concentration increases from 10%wt to 30%wt. However, the decrease is steeper when the concentration of the MEA in the absorbent

solution increases. This trend is related to the fact that the absorption is mainly driven by the MEA molecules. Therefore, when the water concentration increases the MEA concentration decreases. However the total amount of MEA decreases more at a higher concentration of MEA.

In Figure 15 when the water concentration increases from 30%wt to 70%wt the absorption efficiency increases again. This is because here the absorption efficiency is determined by the AMP. As mentioned before during the reaction of AMP with CO_2 there was salt formation, which is soluble in water. Thus, by adding more water, more salt will dissolve. Therefore, the equilibrium of the AMP reaction with the CO_2 will change.

3.1.3. Effect of water concentration and AMP/MEA ratio for nAmine/nCO_2 = 4

The effect of water concentration and AMP/MEA for nAmine/nCO_2 = 4 ratio on the K_Ga_e and the absorption efficiency are shown in Figure 16 and Figure 17. The nAmine/nCO_2 was set at the stochiometric value of 4 and CO_2 concentration was set at 10%vol.

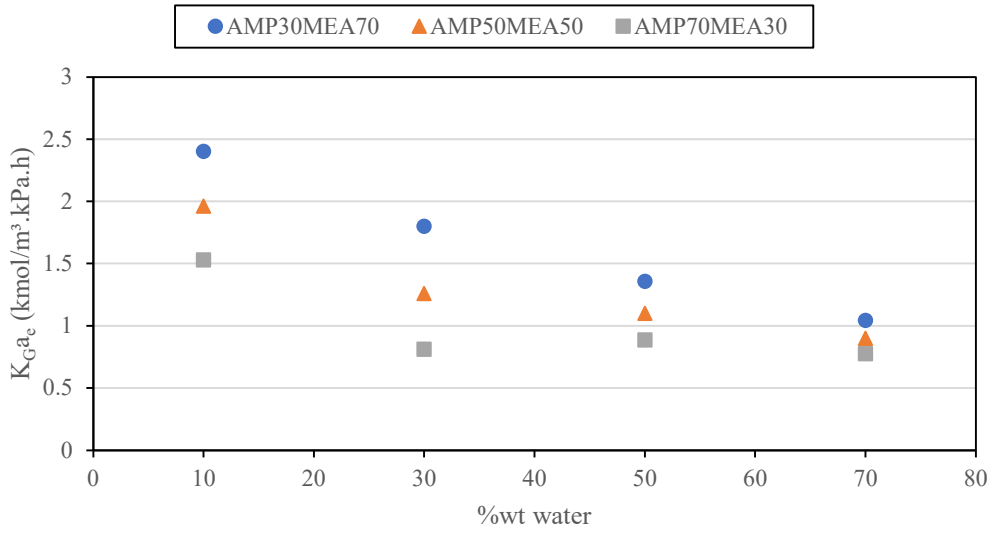

Figure 16: Effect of water %wt and AMP/MEA ratio on K_Ga_e for nAmine/nCO_2 = 4

In Figure 16 the same trends as in Figure 14 are visible. This is expected because only the gas flow rate halved, therefore the ratio nAmine/nCO_2 doubled. All the other input parameters were unchanged. The results of both experiments could not be directly compared because of a difference in gas flow rate and thus a difference in residence time.

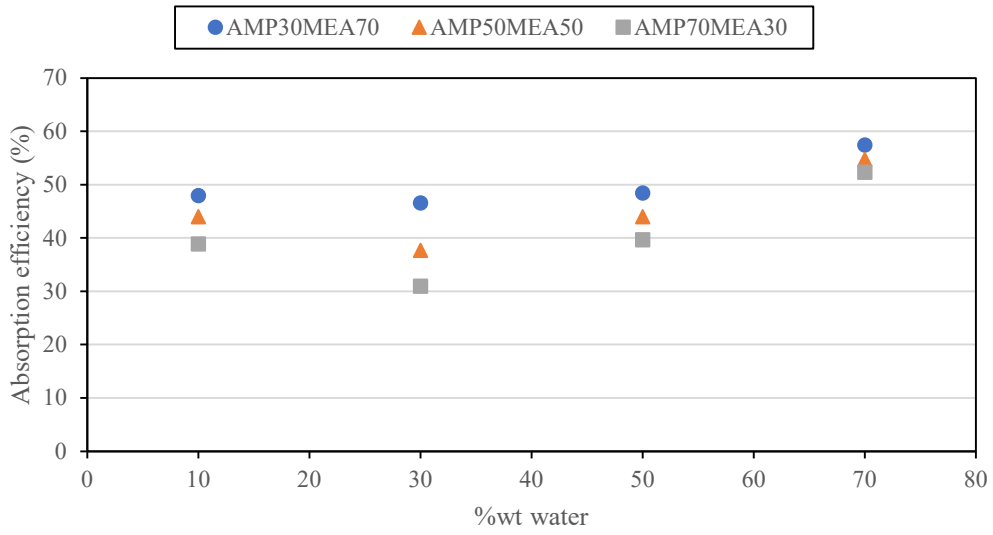

Figure 17: Effect of water %wt and AMP/MEA ratio on absorption efficiency for nAmine/nCO₂ = 4

From Figure 17 the same conclusions as in Figure 15 can be drawn. However, the decrease of the absorption efficiency between the water concentrations 10%wt and 30%wt is less pronounced. This is because nAmine/nCO_2 has doubled. Therefore, there is a double number of moles of MEA per mole of CO_2. This means that if the water concentration is increased the total amount of MEA is less sensible. In Figure 17 the increase of absorption efficiency, when the water concentration is increased from 30%wt to 70%wt, is also observed. This is for the same reason as explained in paragraph 3.1.2Figure 15.

3.1.4. Effect of inlet CO_2 %vol

The effect of inlet CO_2 concentration on the K_Ga_e value and the absorption efficiency are shown in Figure 18 and Figure 19. The experiments were performed at 50 %wt AMP and 50 %wt MEA solutions with 10 %wt water and the nAmine/nCO_2 was set a value of 2.

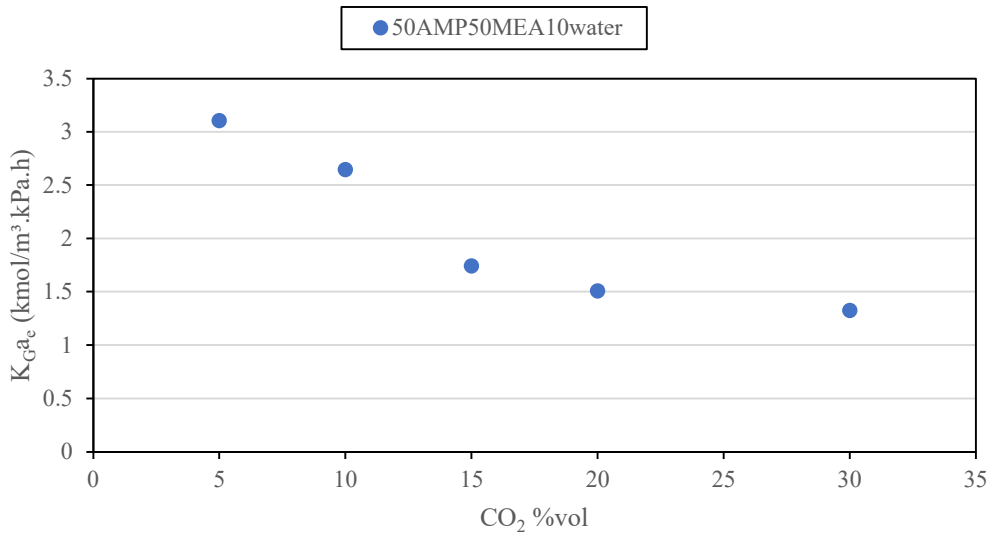

Figure 18: Effect of CO_2 %vol on K_Ga_e

From Figure 18 it can be concluded that the K_Ga_e value decreases when the CO_2 %vol is increased. This is because the molar ratio of the CO_2 is a part of the K_Ga_e equation (equation 8). The curve also flattens when the CO_2 concentration reaches 20 %vol, this could be related to the fact that the amine solutions is already saturated, thus increasing the CO_2 %vol does not affect the K_Ga_e value.

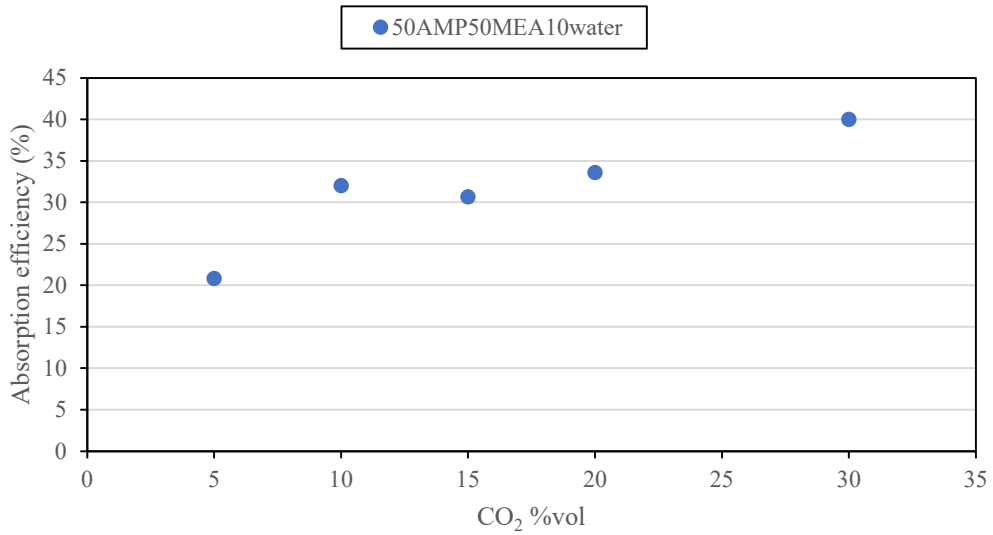

Figure 19: Effect of CO_2 %vol on absorption efficiency

From Figure 19 it can be concluded that the absorption efficiency increases as the CO_2 concentration increases. This due to the salt formation of AMP, when the salt is formed it is diluted in the water, which causes the reaction equilibrium to move and causes a high maximum CO_2 loading. Therefore, when the CO_2 concentration in the gas increases the absorbant liquid does not become saturated, which allows the absorption efficiency to increase.

3.2. Machine Learning modelling K_Ga_e coefficient for CO_2 capture

The ML models predict the K_Ga_e of the CO_2 capture process. The prediction accuracy of the trained ML models will be evaluated against the experimental K_Ga_e values contained in the validation set. For each model the R^2 score, MSE and mean absolute error (MAE) will be evaluated. In this way the models can be compared to each other. The R^2 score is calculated by Equation 19 and the closer the R^2 score of a model is to 1, the higher the accuracy of the model of the model is [44].

$$R^2(y_i, \hat{y}_i) = 1 - \frac{\sum_{i=1}^{n}(y_i - \hat{y}_i)^2}{\sum_{i=1}^{n}(y_i - \bar{y}_i)^2} \quad (19)$$

The MAE is calculated by Equation 20 and the lower the MEA, the better the performance of the model [45].

$$MAE(y_i, \hat{y}_i) = \frac{1}{n_{samples}} * \sum_{i=1}^{n_{samples}} |y_i - \hat{y}_i| \quad (20)$$

The MSE is calculated by Equation 6 and the lower the MSE, the better the performance of the model.

3.2.1. Performance of the ANN model

The performances scores of the trained ANN model are shown in Table 5. The modelled K_Ga_e values of the ANN model and the experimental K_Ga_e are shown in Figure 20 for the validation dataset. The diagonal that is plotted gives the ideal line of predictions.

Table 5: Performance scores of the ANN model

	R^2 score	MSE	MAE
Train	0.933	0.384	0.428
Validation	0.867	0.697	0.523

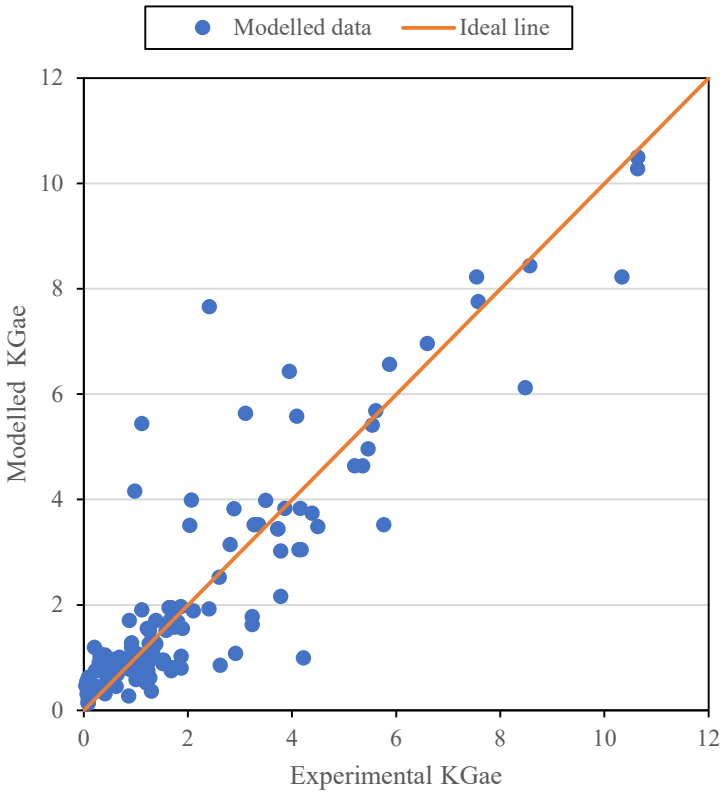

Figure 20: Modelled K_Ga_e validation dataset for ANN model

From Figure 20 it can be concluded that the ANN model is able to capture the trend of the of the experimental K_Ga_e. However, the model is not accurate, at the range of 0-4 experimental K_Ga_e the predictions of the model have a significant deviation compared to the ideal line, which is confirmed by the low R^2 score and the MSE. This can be explained by the deviation in the input dataset, namely not all type of amines have the same amount of data. This causes the model to overfit on certain specific amines solutions. From Table 5 it can be seen that the R^2 score of the training dataset is much higher than the one of the validation dataset and the MSE of the training dataset has even halved in comparison to the validation dataset. In order to further improve the model, the dataset has to be further enriched with new data obtained from the under-represented amine solutions, so that the deviation in amount of data is less.

3.2.2. Performance of the SVR models

The performance scores of the SVR-poly are shown in Table 6. The modelled K_Ga_e values of the SVR-poly and the experimental K_Ga_e are shown in Figure 21 for the validation dataset. The diagonal line of this figure gives the ideal line of predictions.

Table 6: Performance scores of the SVR-poly model

	R^2 score	MSE	MAE
Train	0.958	0.243	0.479
Validation	0.850	0.730	0.291

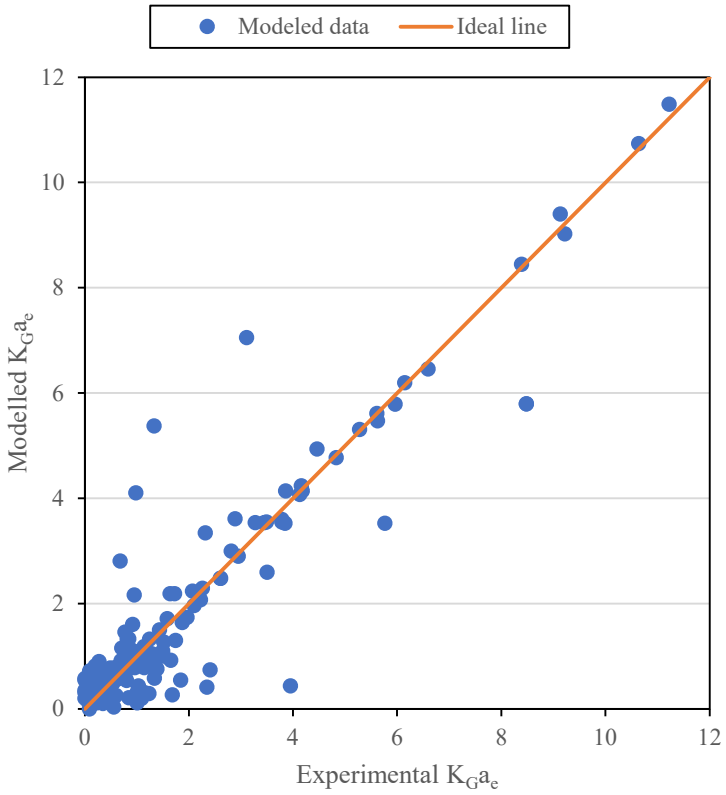

Figure 21: Modelled K_Ga_e validation dataset for SVR-poly model

Figure 21 shows the capabilities of the SVR-poly model in predicting the K_Ga_e. In the range 0-4 experimental K_Ga_e, the model predicts some points that have a much higher or much lower value than the ideal line. This causes the MSE to increases and the R^2 score to decrease. This again can be explained by the uneven distribution of the dataset, where the number of data points for some amine solutions are low. This is confirmed by the performance scores of Table 6. The R^2 score of the model is close to 1 and both the MSE and MAE are low in comparison to the order of magnitude than the K_Ga_e values. Thus, it can be concluded that the SVR-poly is able to accurately model the CO_2 capture process.

The performance scores of the SVR-lin are shown in Table 7. The modelled K_Ga_e values of the SVR-lin and the experimental K_Ga_e are shown in **Error! Reference source not found.** for the validation dataset. The diagonal that is plotted gives the ideal line of prediction.

Table 7: Performance scores of the SVR lin-model

	R^2 score	MSE	MAE
Train	0.684	1.806	0.881
Validation	0.644	1.737	0.881

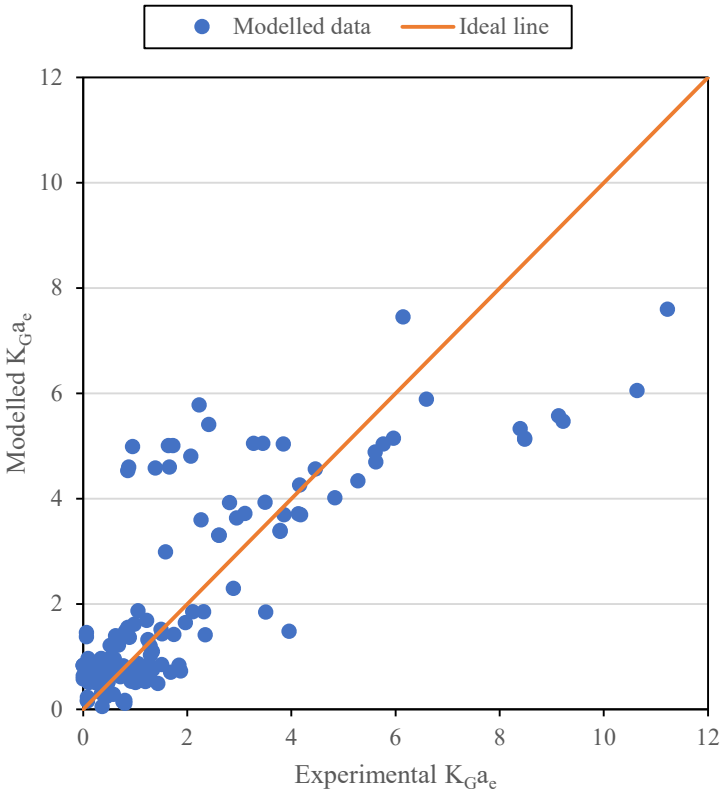

Figure 22: Modelled K_Ga_e validation dataset for SVR lin-model

In Figure 22, within the range of 0-4 experimental K_Ga_e, the modelled values show an high deviation from the ideal prediction line. In the range of 2-8 the predicted values are in general above the ideal prediction line. In the range of 8-12 experimental K_Ga_e, the modelled values are always below the ideal line values. This causes the high MSE for this modelling technique and it can be concluded that the SVR-lin is not able to accurately predict the K_Ga_e. The poor prediction accuracies are related to the fact that the model heavily relies on linear kernel transformation that, in this case, drastically reduce the accuracy because of the strongly non-linear behavior of the system.

The performance scores of the SVR-rbf are shown in Table 8. The modelled K_Ga_e values of the SVR-rbf and the experimental K_Ga_e are shown in Figure 23 for the validation dataset. The diagonal that is plotted gives the ideal line of prediction.

Table 8: Performance scores of the SVR-rbf model

	R^2 score	MSE	MAE
Train	0.941	0.339	0.493
Validation	0.837	0.794	0.330

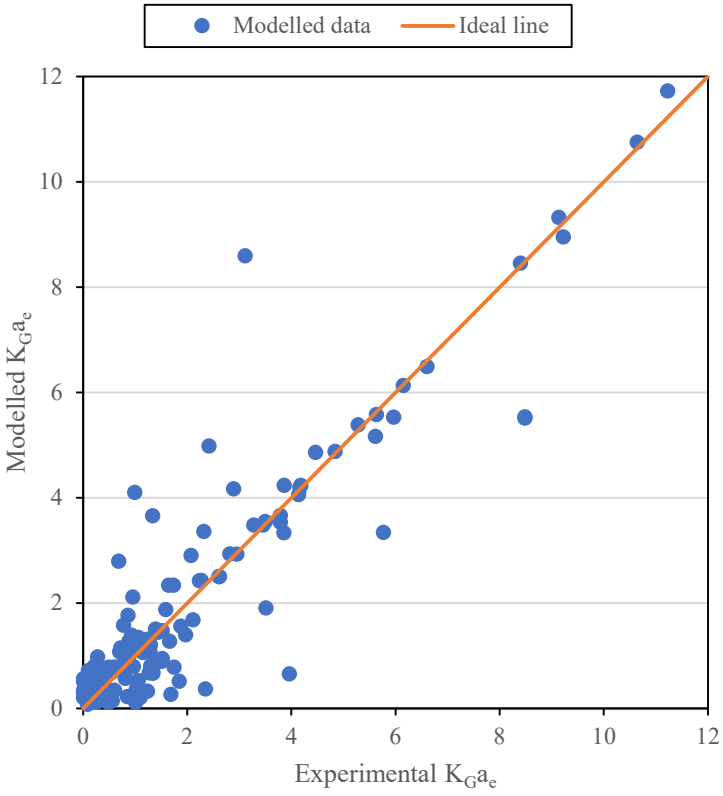

Figure 23: Modelled K_Ga_e validation dataset for SVR-rbf model

From Figure 23 it can be concluded that the trained SVR-rbf model accurately predicts the K_Ga_e. In the range of 0-4 experimental K_Ga_e the modelled values are higher than the ideal line, this causes the higher MSE. There are also a few outliers, from which the modelled values are lower than the ideal line. This can be explained by the uneven distribution of the dataset and the model is unable to catch this deviation in input parameters. This accuracy is confirmed by the performance scores of Table 8. The R^2 score is close to 1 and the MSE and MAE are both one order of magnitude lower than the K_Ga_e. Based on these metrics and on Figure 23 Table 9 it can be concluded that the SVR-rbf can accurately model the CO_2 capture process.

In Table 9 the performance scores of the three SVR models are compared for the validation dataset.

Table 9: Performance scores of the SVR models for validation dataset

	Validation set		
Model name	R^2 score	MSE	MAE
SVR-poly	0.850	0.730	0.291
SVR-lin	0.644	1.737	0.881
SVR-rbf	0.837	0.794	0.330

Table 9 reports a lower MSE and MAE for the SVR-poly and SVR-rbf model, however the SVR-lin has a much higher MSE and MAE than the other two models. The same can be detected for the R^2 score, where the score of the SVR-poly and SVR-rbf is closer to 1 than the score of the SVR-lin model. Therefore, it can be concluded that the SVR-poly and the SVR-rbf are both accurate models of the CO_2 capture.

3.2.3. Performance of the DTR model

The performance scores of the DTR model is shown in Table 10 and the modelled K_Ga_e for the validation dataset is shown in Figure 24.

Table 10: Performance scores of the DTR model

	R^2 score	MSE	MAE
Train	0.838	0.925	0.618
Validation	0.809	1.00	0.648

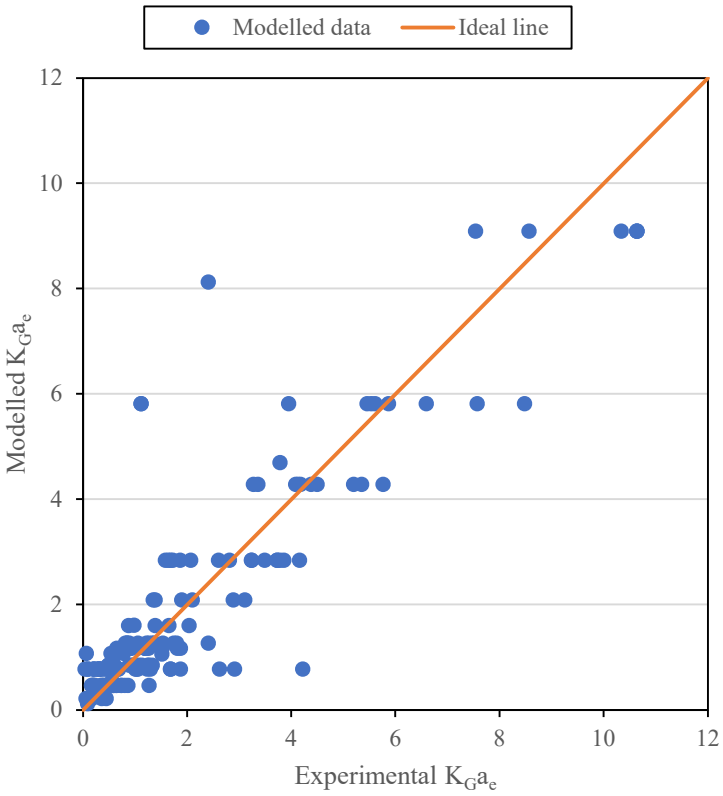

Figure 24: Modelled K_Ga_e over the validation dataset for DTR model

The performance scores of the DTR are comparable to the performance scores of the SVR-poly and the SVR-rbf. However, from Figure 24 the DTR model cannot accurately predict the K_Ga_e coefficient. The DTR has a limit amount of output values, due to the limited number of leaf nodes. This is because a 10-fold cross validation was used for the hyperparameter tuning and by increasing the number of leaves the model would overfit on the training dataset. Therefore, different levels of modelled K_Ga_e can be seen on Figure 24. It can be concluded that the DTR model is not usable for modelling the K_Ga_e of the CO_2 capture process.

3.2.4. Comparison of performance of different models

The SVR-poly is the most accurate model out of the five models tested in this thesis work. The SVR-rbf is also accurate but the prediction performances are inferior to the SVR-poly. This conformed by the lower R^2 score of the SVR-rbf model and the higher MSE. The ANN model shows potential in the performance scores of the training dataset but is not accurate when applied on the validation dataset. The SVR-lin is not accurate, because of the non-linear relationship in the training dataset. Finally, the DTR is model is not accurate, this is because of its limit amount of output values.

The SVR-poly and the SVR-rbf kernel function both have a high R^2 score and a low MSE and thus they are both accurate and robust models. The validation dataset, just as the training dataset, consists of three different types of amines and seven different mixtures of these amines. These datapoints were collected on both a spray column and a packed column and had a wide variety of different input features, such as CO_2 %vol, gas flow rate and liquid flow rate. Beside the various input features and capture technologies, the model was trained with different solutions of amines both in concentration and components. This means that the model trained in this work is highly flexible both on process condition, capture technology

and absorbent solutions. Despite this wide variety in the utilized datasets, SVR-poly and SVR-rbf models can accurately predict the K_Ga_e coefficient.

4. Conclusion and future work

The aim of this thesis is to model the CO_2 absorption performance of packed and spray columns utilizing Machine Learning techniques. The models utilizes as input: the process conditions, information about the columns and information about the absorbent liquid. The Machine Learning technique models require data to be developed. In this work the data were collected both from literature data and lab experiments.

The lab experiment focused on the absorbent mixture AMP-MEA-water. From the lab experiments was found that when the water concentration is low, namely in the range from 10%wt to 50%wt, the K_Ga_e and the absorption efficiency are mainly influenced by the MEA and both the values decreased by increasing the water concentration. In the range of water concentration from 50%wt to 70%wt the K_Ga_e and the absorption efficiency are mainly influenced by the AMP concentration and both values increases with the water concentration. This trend is caused by a salt formation between CO_2 and AMP, which is soluble in water. When the CO_2 concentration in the gas increases, the K_Ga_e decreases but the absorption efficiency increases.

The Machine Learning techniques used in this thesis were ANN, SVR and DTR. With these techniques, five different models were trained in this thesis, using training data that consisted of different MEA, AMP, MDEA and Water mixtures. The most accurate model detected in this thesis employs SVR regressor with polynomial kernel function (i.e. SVR-poly) with the highest R^2 score and lowest MSE and MAE for the validation dataset observed in this work. The SVR-lin model is not accurate, this is because it cannot capture the non-linear relationships between the input features and the output. The SVR-rbf model is also an accurate model with a high R^2 score and a low MSE and MAE for the validation dataset. The ANN model shows a lot of potential based on the training dataset, namely the R^2 score is high and the MSE is low. However, when the validation dataset is applied on the ANN model the performance is not good and the R^2 score is low and the MSE is high. This leads to the conclusion that the ANN model is not accurate and suffers from over-fitting problems over the training set. The last model is the DTR model, this model was not able to accurately predict the K_Ga_e values, because DTR has a limited amount of output values.

Finally, it can be concluded that a ML model is able to accurately predict the K_Ga_e coefficient for CO_2 capture in both a spray and packed column with a wide variety of input parameters. Besides the various input parameters and capture technology the model can make prediction over several different amine solutions. This means that the model trained in this thesis is highly flexible both on process condition, spray technology and absorbent solutions.

To further generalize the capabilities of the model in future work the dataset can be enriched with more types of amines and more operating conditions. A further development in the model structure is the usage of Graph Neural Network structure, which could also increases the generalization capabilities of the model.

Bibliograph

[1] IPCC, *Technical Summary. Contribution of Working Group I to the Sixth Assessment Report of the Intergovernmental Panel on Climate Change*. 2021.

[2] H. Yang *et al.*, "Progress in carbon dioxide separation and capture: A review," *Journal of Environmental Sciences*, vol. 20, no. 1, pp. 14–27, Jan. 2008, doi: 10.1016/S1001-0742(08)60002-9.

[3] S. M. Benson and F. M. Orr, "Carbon dioxide capture and storage," *MRS Bulletin*, vol. 33, no. 4, pp. 303–305, 2008, doi: 10.1557/mrs2008.63.

[4] J. Kuntz and A. Aroonwilas, "Mass transfer in a spray column for CO2 removal," *2006 IEEE EIC Climate Change Technology Conference, EICCCC 2006*, no. 306, pp. 0–5, 2006, doi: 10.1109/EICCCC.2006.277211.

[5] J. Kuntz and A. Aroonwilas, "Mass-transfer efficiency of a spray column for CO2 capture by MEA," *Energy Procedia*, vol. 1, no. 1, pp. 205–209, Feb. 2009, doi: 10.1016/J.EGYPRO.2009.01.029.

[6] R. R. Wanderley, D. D. D. Pinto, and H. K. Knuutila, "From hybrid solvents to water-lean solvents – A critical and historical review," *Separation and Purification Technology*, vol. 260, p. 118193, Apr. 2021, doi: 10.1016/J.SEPPUR.2020.118193.

[7] S. Santos, J. Gomes, and J. Bordado, "Scale-Up Effects of CO2 Capture by Methyldiethanolamine (MDEA) Solutions in Terms of Loading Capacity," *Technologies (Basel)*, vol. 4, no. 3, p. 19, 2016, doi: 10.3390/technologies4030019.

[8] C. H. Yu, C. H. Huang, and C. S. Tan, "A review of CO2 capture by absorption and adsorption," *Aerosol and Air Quality Research*, vol. 12, no. 5, pp. 745–769, 2012, doi: 10.4209/aaqr.2012.05.0132.

[9] N. Sipöcz, F. A. Tobiesen, and M. Assadi, "The use of Artificial Neural Network models for CO2 capture plants," *Applied Energy*, vol. 88, no. 7, pp. 2368–2376, Jul. 2011, doi: 10.1016/J.APENERGY.2011.01.013.

[10] Q. Zhang, R. Turton, and D. Bhattacharyya, "Development of Model and Model-Predictive Control of an MEA-Based Postcombustion CO2 Capture Process," *Industrial and Engineering Chemistry Research*, vol. 55, no. 5. pp. 1292–1308, 2016. doi: 10.1021/acs.iecr.5b02243.

[11] N. Razi, H. F. Svendsen, and O. Bolland, "Assessment of mass transfer correlations in rate-based modeling of a large-scale CO2 capture with MEA," *International Journal of Greenhouse Gas Control*, vol. 26, pp. 93–108, Jul. 2014, doi: 10.1016/j.ijggc.2014.04.019.

[12] Y. Xu, X. Chen, Y. Zhao, and B. Jin, "Modeling and analysis of CO2 capture by aqueous ammonia + piperazine blended solution in a spray column," *Separation and Purification Technology*, vol. 267, p. 118655, Jul. 2021, doi: 10.1016/J.SEPPUR.2021.118655.

[13] *Machine Learning in Radiation Oncology*. 2015. doi: 10.1007/978-3-319-18305-3.

[14] P. P. Shinde and S. Shah, “A Review of Machine Learning and Deep Learning Applications,” *Proceedings - 2018 4th International Conference on Computing, Communication Control and Automation, ICCUBEA 2018*, 2018, doi: 10.1109/ICCUBEA.2018.8697857.

[15] M. R. Dobbelaere, P. P. Plehiers, R. van de Vijver, C. v. Stevens, and K. M. van Geem, “Machine Learning in Chemical Engineering: Strengths, Weaknesses, Opportunities, and Threats,” *Engineering*, vol. 7, no. 9, pp. 1201–1211, Sep. 2021, doi: 10.1016/J.ENG.2021.03.019.

[16] A. M. Schweidtmann *et al.*, “Machine Learning in Chemical Engineering: A Perspective,” *Chemie-Ingenieur-Technik*, vol. 93, no. 12, pp. 2029–2039, 2021, doi: 10.1002/cite.202100083.

[17] P. Zhang, “Industrial control system simulation routines,” *Advanced Industrial Control Technology*, pp. 781–810, Jan. 2010, doi: 10.1016/B978-1-4377-7807-6.10019-1.

[18] O. I. Abiodun, A. Jantan, A. E. Omolara, K. V. Dada, N. A. E. Mohamed, and H. Arshad, “State-of-the-art in artificial neural network applications: A survey,” *Heliyon*, vol. 4, no. 11, p. e00938, Nov. 2018, doi: 10.1016/J.HELIYON.2018.E00938.

[19] Y.-C. Wu and J.-W. Feng, “Development and Application of Artificial Neural Network,” *Wireless Personal Communications*, vol. 102, doi: 10.1007/s11277-017-5224-x.

[20] C. Engineering, “Modeling and Experimental Study of Carbon Dioxide Absorption in a Membrane Contactor,” *Science And Technology*, no. 3399, 2003.

[21] G. Chen *et al.*, “Artificial neural network models for the prediction of CO2 solubility in aqueous amine solutions,” *International Journal of Greenhouse Gas Control*, vol. 39, pp. 174–184, 2015, doi: 10.1016/j.ijggc.2015.05.005.

[22] M. Rahimi, S. M. Moosavi, B. Smit, and T. A. Hatton, “Toward smart carbon capture with machine learning,” *Cell Reports Physical Science*, vol. 2, no. 4, p. 100396, 2021, doi: 10.1016/j.xcrp.2021.100396.

[23] X. Wu, J. Shen, M. Wang, and K. Y. Lee, “Intelligent predictive control of large-scale solvent-based CO2 capture plant using artificial neural network and particle swarm optimization,” *Energy*, vol. 196, p. 117070, Apr. 2020, doi: 10.1016/J.ENERGY.2020.117070.

[24] N. Daneshvar, M. T. Zaafarani Moattar, M. Abedinzadegan Abdi, and S. Aber, “Carbon dioxide equilibrium absorption in the multi-component systems of CO2 + TIPA + MEA + H2O, CO2 + TIPA + Pz + H2O and CO2 + TIPA + H2O at low CO2 partial pressures: experimental solubility data, corrosion study and modeling with artificial neural network,” *Separation and Purification Technology*, vol. 37, no. 2, pp. 135–147, Jun. 2004, doi: 10.1016/J.SEPPUR.2003.09.004.

[25] H. Saghafi and M. Arabloo, “Modeling of CO2 solubility in MEA, DEA, TEA, and MDEA aqueous solutions using AdaBoost-Decision Tree and Artificial Neural Network,” *International Journal of Greenhouse Gas Control*, vol. 58, pp. 256–265, Mar. 2017, doi: 10.1016/J.IJGGC.2016.12.014.

[26] W. S. Noble, “What is a support vector machine?,” 2006. [Online]. Available: http://www.nature.com/naturebiotechnology

[27] R. Gholami and N. Fakhari, “(No Title),” 2017, doi: 10.1016/B978-0-12-811318-9.00027-2.

[28] R. Burbidge, M. Trotter, B. Buxton, and S. Holden, “Drug design by machine learning: support vector machines for pharmaceutical data analysis,” *Computers & Chemistry*, vol. 26, no. 1, pp. 5–14, Dec. 2001, doi: 10.1016/S0097-8485(01)00094-8.

[29] I. Yélamos, G. Escudero, M. Graells, and L. Puigjaner, “Performance assessment of a novel fault diagnosis system based on support vector machines,” *Computers & Chemical Engineering*, vol. 33, no. 1, pp. 244–255, Jan. 2009, doi: 10.1016/J.COMPCHEMENG.2008.08.008.

[30] Y. Li, H. Wang, K. Bai, and S. Chen, “Dynamic intelligent risk assessment of hazardous chemical warehouse fire based on electrostatic discharge method and improved support vector machine,” *Process Safety and Environmental Protection*, vol. 145, pp. 425–434, Jan. 2021, doi: 10.1016/J.PSEP.2020.11.012.

[31] R. Nakhaei-Kohani, E. Taslimi-Renani, F. Hadavimoghaddam, M.-R. Mohammadi, and A. Hemmati-Sarapardeh, “Modeling solubility of CO 2-N 2 gas mixtures in aqueous electrolyte systems using artificial intelligence techniques and equations of state,” *Scientific Reports* |, vol. 12, p. 3625, 123AD, doi: 10.1038/s41598-022-07393-z.

[32] Z. Li, D. Wu, and T. Yu, “Prediction of Material Removal Rate for Chemical Mechanical Planarization Using Decision Tree-Based Ensemble Learning,” vol. 141, no. March, pp. 1–14, 2019, doi: 10.1115/1.4042051.

[33] H. Yarveicy, H. Saghafi, M. M. Ghiasi, and A. H. Mohammadi, “Decision tree-based modeling of CO 2 equilibrium absorption in different aqueous solutions of absorbents,” *Environmental Progress and Sustainable Energy*, vol. 38, no. s1, pp. S441–S448, 2019, doi: 10.1002/ep.13128.

[34] H. Saghafi and M. Arabloo, “Modeling of CO2 solubility in MEA, DEA, TEA, and MDEA aqueous solutions using AdaBoost-Decision Tree and Artificial Neural Network,” *International Journal of Greenhouse Gas Control*, vol. 58, pp. 256–265, 2017, doi: 10.1016/j.ijggc.2016.12.014.

[35] A. van den Bogaert, “A parametric study on CO2 capture with aqueous monoethanolamine solutions in a spray reactor,” KULeuven, 2021.

[36] A. Setameteekul and R. Saskatchewan, “Statistical factorial design analysis of mass-transfer in CO2 absorption using MEA and MEA/MDEA,” University of Regina, 2006.

[37] A. Dey, “Study of C02 Absorption in Blended Aqueous Monoethanolamine and 2-Amino-2-methyl-l-propanol,” 2008.

[38] “No Title.” https://scikit-learn.org/stable/modules/classes.html#module-sklearn.preprocessing

[39] “No Title.” https://pytorch.org/

[40] S. Jang and Y. Son, “Empirical Evaluation of Activation Functions and Kernel Initializers on Deep Reinforcement Learning,” *ICTC 2019 - 10th International Conference on ICT Convergence: ICT Convergence Leading the Autonomous Future*, pp. 1140–1142, 2019, doi: 10.1109/ICTC46691.2019.8939854.

[41] T. Fushiki, “Estimation of prediction error by using K-fold cross-validation,” *Statistics and Computing*, vol. 21, no. 2, pp. 137–146, 2011, doi: 10.1007/s11222-009-9153-8.

[42] F. Barzagli, M. di Vaira, F. Mani, and M. Peruzzini, “Improved solvent formulations for efficient CO2 absorption and low-temperature desorption,” *ChemSusChem*, vol. 5, no. 9, pp. 1724–1731, 2012, doi: 10.1002/cssc.201200062.

[43] R. Sakwattanapong, A. Aroonwilas, and A. Veawab, “Reaction rate of CO2 in aqueous MEA-AMP solution: Experiment and modeling,” *Energy Procedia*, vol. 1, no. 1, pp. 217–224, Feb. 2009, doi: 10.1016/J.EGYPRO.2009.01.031.

[44] “No Title.” https://scikit-learn.org/stable/modules/model_evaluation.html#r2-score

[45] “No Title.” https://scikit-learn.org/stable/modules/model_evaluation.html#mean-absolute-error

[46] L. Dubois and D. Thomas, “Carbon dioxide absorption into aqueous amine based solvents: Modeling and absorption tests,” *Energy Procedia*, vol. 4, pp. 1353–1360, 2011, doi: 10.1016/j.egypro.2011.01.194.

[47] A. Henni, P. Tontiwachwuthikul, and A. Chakma, “Volumetric properties and viscosities for aqueous NFM solutions from 25°C to 70°C,” *Journal of Chemical and Engineering Data*, vol. 49, no. 6, pp. 1724–1726, 2004, doi: 10.1021/je0498208.

[48] U. S. P. R. Arachchige, N. Aryal, D. A. Eimer, and M. C. Melaaen, “Viscosities of Pure and Aqueous Solutions of Monoethanolamine (MEA), Diethanolamine (DEA) and N-Methyldiethanolamine (MDEA),” *Annual Transactions of the Nordic Rheology Society*, vol. 21, pp. 299–306, 2013.

[49] E. Álvarez, Á. Cancela, R. Maceiras, J. M. Navaza, and R. Táboas, “Surface tension of aqueous binary mixtures of 1-amino-2-propanol and 3-amino-1-propanol, and aqueous ternary mixtures of these amines with diethanolamine, triethanolamine, and 2-amino-2-methyl-1-propanol from (298.15 to 323.15) K,” *Journal of Chemical and Engineering Data*, vol. 48, no. 1, pp. 32–35, 2003, doi: 10.1021/je020048n.

[50] N. S. Mousavi, B. Vaferi, and A. Romero-Martínez, “Prediction of Surface Tension of Various Aqueous Amine Solutions Using the UNIFAC Model and Artificial Neural Networks,” *Industrial and Engineering Chemistry Research*, vol. 60, no. 28, pp. 10354–10364, 2021, doi: 10.1021/acs.iecr.1c01048.

[51] G. F. Versteeg and W. P. M. van Swaal, “Solubility and Diffusivity of Acid Gases (CO2, N2O) in Aqueous Alkanolamine Solutions,” *Journal of Chemical and Engineering Data*, vol. 33, no. 1, pp. 29–34, 1988, doi: 10.1021/je00051a011.

Appendix

Appendix list

A.1. Operating conditions and results of experiments

In this section the operating conditions and results of the lab experiments done in this thesis are shown.

Am1	Am2	wAmine1 [%wt]	wAmine2 [%wt]	wWater [%wt]	CO2 conc [%vol]	Liquid Fr [mL.min^{-1}]	Gas Fr [L.min^{-1}]	K_Ga_e [kmol.m^{-3}.kPa^{-1}.h^{-1}]
AMP	NONE	0	5	10	0.5	9.5	10	25.3
AMP	NONE	0	5	10	2.35	44.65	47	108.8
AMP	NONE	0	5	10	1.175	22.325	23.5	0.0
AMP	NONE	70	10	5	0.18	1.62	1.8	78.5
AMP	NONE	50	10	5	0.3	2.7	3	62.6
AMP	NONE	70	5	3.14	0.74	14.06	14.8	121.7
AMP	NONE	70	5	5	0.075	1.425	1.5	40.6
AMP	NONE	70	5	5	0.09	1.71	1.8	47.8
AMP	NONE	70	5	5	0.125	2.375	2.5	58.1
AMP	NONE	70	5	8	0.1	1.9	2	32.3
AMP	NONE	70	5	10	0.105	1.995	2.1	23.0
AMP	NONE	70	5	10	0.74	14.06	14.8	33.7
AMP	NONE	70	5	13	0.48	9.12	9.6	24.7
AMP	NONE	70	5	10	0.09	1.71	1.8	25.3
AMP	NONE	70	15	10	0.375	2.125	2.5	65.5
AMP	NONE	70	12.5	10	0.3625	2.5375	2.9	47.1
AMP	MEA	0	10	10	0.1	0.9	1	17.0
AMP	MEA	0	10	10	0.93	8.37	9.3	84.7
AMP	MEA	0	5	10	0.05	0.95	1	8.9
AMP	MEA	0	10	10	0.1	0.9	1	16.5
AMP	MEA	0	5	10	0.1	1.9	2	17.8
AMP	MEA	0	5	10	0.055	1.045	1.1	9.2
AMP	MEA	0	5	10	0.05	0.95	1	8.8
AMP	MEA	0	5	10	0.15	2.85	3	22.4
AMP	MEA	0	5	10	0.045	0.855	0.9	7.9
AMP	MEA	0	5	10	0.165	3.135	3.3	24.9
AMP	MEA	0	5	10	0.165	3.135	3.3	24.9
AMP	MEA	0	5	10	1.64	31.16	32.8	142.3
AMP	MEA	0	5	10	0.14	2.66	2.8	20.5
AMP	NONE	0	10	10	0.039	0.351	0.39	8.4
AMP	NONE	0	10	10	0.12	1.08	1.2	0.1
AMP	MEA	0	10	10	0.16	1.44	1.6	19.6
MDEA	NONE	30	5	10	1.35	25.65	27	0.0
MDEA	NONE	0	10	10	0.1	0.9	1	1.2
MDEA	MEA	0	5	10	0.055	1.045	1.1	0.0
MDEA	MEA	0	5	10	0.16	3.04	3.2	27.2
MDEA	MEA	0	5	10	0.045	0.855	0.9	0.0
MDEA	MEA	0	5	10	0.14	2.66	2.8	6.6
MEA	NONE	70	10	10	0.2	1.8	2	59.0
MEA	NONE	0	10	2.5	0.93	8.37	9.3	101.2

MEA	NONE	0	10	5	0.93	8.37	9.3	202.8
MEA	NONE	0	10	10	0.1	0.9	1	13.7
MEA	NONE	0	10	10	0.93	8.37	9.3	119.7
MEA	NONE	0	10	15	0.93	8.37	9.3	83.2
MEA	NONE	0	10	20	0.93	8.37	9.3	63.5
AMP	MEA	70	10	10	0.00088 4	0.007958	0.008843	0.2
AMP	MEA	50	10	10	0.00147 1	0.013238	0.014709	0.1
AMP	MEA	30	10	10	0.00205 5	0.018497	0.020552	0.1
AMP	MEA	10	10	10	0.00263 7	0.023734	0.026371	0.2
AMP	MEA	70	10	10	0.00081 9	0.007371	0.00819	0.2
AMP	MEA	50	10	10	0.00135 8	0.012223	0.013581	0.1
AMP	MEA	30	10	10	0.00189 2	0.017026	0.018917	0.1
AMP	MEA	10	10	10	0.00242	0.021778	0.024198	0.1
AMP	MEA	70	10	10	0.00075 4	0.006789	0.007543	0.2
AMP	MEA	50	10	10	0.00124 7	0.011223	0.01247	0.1
AMP	MEA	30	10	10	0.00173 1	0.015583	0.017314	0.1
AMP	MEA	10	10	10	0.00220 8	0.019868	0.022076	0.1
AMP	MEA	50	10	10	0.00124 7	0.011223	0.01247	0.1
AMP	MEA	30	10	10	0.00173 1	0.015583	0.017314	0.1
AMP	MEA	10	10	10	0.00220 8	0.019868	0.022076	0.1
AMP	MEA	10	5	10	0.00242	0.045977	0.048397	0.1
AMP	MEA	10	10	10	0.00242	0.021778	0.024198	0.2
AMP	MEA	10	15	10	0.00242	0.013712	0.016132	0.2
AMP	MEA	10	20	10	0.00242	0.009679	0.012099	0.2
AMP	MEA	10	30	10	0.00242	0.005646	0.008066	0.2
AMP	MEA	70	10	10	0.00044 2	0.003979	0.004421	0.1
AMP	MEA	50	10	10	0.00073 5	0.006619	0.007354	0.1
AMP	MEA	30	10	10	0.00102 8	0.009248	0.010276	0.1
AMP	MEA	10	10	10	0.00131 9	0.011867	0.013186	0.1
AMP	MEA	70	10	10	0.00041	0.003686	0.004095	0.1
AMP	MEA	50	10	10	0.00067 9	0.006112	0.006791	0.1
AMP	MEA	30	10	10	0.00095	0.008513	0.009459	0.1
AMP	MEA	10	10	10	0.00121	0.010889	0.012099	0.1
AMP	MEA	70	10	10	0.00038	0.003395	0.003772	0.3

AMP	MEA	50	10	10	0.000623	0.005611	0.006235	0.3
AMP	MEA	30	10	10	0.000866	0.007791	0.008657	0.3
AMP	MEA	10	10	10	0.001104	0.009934	0.011038	0.3

A.2. Chemical properties

In this section the chemical properties of the amines and water, that were used by each model are shown.

Chemical	**Density [g.cm^{-3}]**	**Source**
MEA	1.01	[46]
AMP	0.930	[47]
MDEA	1.04	[46]
Water	1	
Chemical	**Dynamic viscosity [mPa.s]**	**Source**
MEA	15.1	[48]
AMP	99.2	[47]
MDEA	57.8	[48]
Water	0.986	[46]
Chemical	**Kinematic viscosity [cm^2.s^{-1}]**	**Source**
MEA	15.0	[46]
AMP	107	[46]
MDEA	55.6	[46]
Water	0.986	[46]
Chemical	**Surface tension [mN.m^{-1}]**	**Source**
MEA	47.5	Measurement by previous work research group CIPT
AMP	70.42	[49]
MDEA	37.62	[50]
Water	72	Measurement by previous work research group CIPT
Chemical	**Diffusion coefficient [m^2.s^{-1}]**	**Source**
MEA	1.25E-10	Calculated by using equation of Versteeg et al. [51]
AMP	9.86E-04	Calculated by using equation of Versteeg et al. [51]
MDEA	1.91E-11	Calculated by using equation of Versteeg et al. [51]
Water	3.28E-11	Calculated by using equation of Versteeg et al. [51]